

A note to editor and reviews regarding update in Supplementary Material:

Dear editor and reviewers,

Regarding the question by Reviewer #1 on the assumption of $Q_{s,ambient}=Q_{s,dry}$ in the $f(RH)_{water}$ equation derivation, we responded that the $Q_{s,ambient}/Q_{s,dry}$ ratio was on average 1.40. We recalculated this ratio, considering variations in refractive index and using a broader range of particle sizes in the distribution, and found the ratio to be on average 1.06 for the SOAS study, and with a relative bias in $f(RH)_{water}$ of 10%. This is discussed in the main body of the manuscript, and detailed in the Supplementary Material Section 2 accordingly.

1 **Particle**~~Particle~~Fine particle water and pH in the southeastern United States

Style Definition: Heading 3: Font: Italic

2 Hongyu Guo¹, Lu Xu², Aikaterini Bougiatioti^{2,8}, Kate M. Cerully^{2*}, Shannon L. Capps^{4,§}, James R.
3 ~~Hite~~[†]Hite Jr.[†], Annmarie G. Carlton⁵, Shan-Hu Lee⁶, Michael H. Bergin^{1,3}, Nga L. Ng^{1,2}, Athanasios
4 Nenes^{1,2,7,†}, and Rodney J. Weber^{1,†}

5 ¹ School of Earth and Atmospheric Sciences, Georgia Institute of Technology, Atlanta, GA, USA

6 ² School of Chemical and Biomolecular Engineering, Georgia Institute of Technology, Atlanta, GA, USA

7 ³ School of Civil & Environmental Engineering, Georgia Institute of Technology, Atlanta, GA, USA

8 ⁴ Office of Research and Development, United States Environmental Protection Agency, Research
9 Triangle Park, NC, USA

10 ⁵ Department of Environmental Sciences, Rutgers University, New Brunswick, NJ, USA

11 ⁶ College of Public Health, Kent State University, Kent, Ohio, USA

12 ⁷ Foundation for Research and Technology, Hellas, Greece

13 ⁸ National Technical University of Athens, Athens, Greece

14 ^{*}Now at TSI, Inc., Shoreview, MN, USA

Formatted: Superscript

15 [§]Now at Department of Mechanical Engineering, University of Colorado Boulder, Boulder, CO, USA

16 [†]Corresponding Author: R. Weber and A. Nenes, (rodney.weber@eas.gatech.edu;
17 athanasios.nenes@gatech.edu)

18 **Abstract**

19 Particle water and pH are predicted using ~~thermodynamic modeling (with ISORROPIA-II);~~
20 meteorological observations (RH, T), ~~and gas/particle composition;~~ and thermodynamic modeling
21 (ISORROPIA-II). A comprehensive uncertainty analysis is included, ~~and the model is validated with~~
22 ~~ammonia partitioning. The method is applied to predict.~~ We investigate mass concentrations of particle
23 water and related particle pH for ambient fine mode aerosols sampled in a relatively remote Alabama
24 forest during the Southern Oxidant and Aerosol Study (SOAS) in summer; and at various sites in the
25 southeastern US; during different seasons, as part of the Southeastern Center for Air Pollution and
26 Epidemiology (SCAPE) study. Particle water and pH are closely linked; pH is a measure of the particle
27 H^+ aqueous concentration; ~~and so~~ depends on both the presence of ions and amount of particle liquid
28 water. Levels of particle water, in-turn, are determined through water uptake by both the ionic species and
29 organic compounds. ~~Particle ion balances, often used to infer pH, do not consider either the dissociation~~
30 ~~state of individual ions, nor particle liquid water levels and so do not necessarily correlate with particle~~
31 ~~pH.~~ Thermodynamic calculations based on measured ion concentrations can predict both pH and liquid
32 water; ~~but do not consider~~ may be biased since contributions of organic species to liquid water ~~and so may~~
33 ~~also be biased.~~ are not considered. In this study, contributions of both the inorganic and organic fractions
34 to aerosol liquid water were considered and predictions were in good agreement with measured liquid
35 water based on differences in ambient and dry light scattering coefficients (prediction vs. measurement:
36 slope = 0.91, intercept = 0.4546 $\mu\text{g m}^{-3}$, $R^2 = 0.8775$). ISORROPIA-II predictions were
37 ~~evaluated~~ confirmed by ~~reproducing the observed gas-particle partitioning of NH_3 ;~~ good agreement
38 between predicted and measured ammonia concentrations (slope = 1.07, intercept = -0.12 $\mu\text{g m}^{-3}$, $R^2 =$
39 0.76). Based on this study, organic species on average contributed 35% to the total water, with a
40 substantially higher contribution (~~63~~50%) at night. ~~However, not~~ The mean pH predicted in the Alabama
41 ~~forest (SOAS) was 0.94 ± 0.59 (median 0.93).~~ ~~Not~~ including contributions of organic water ~~has had~~ a
42 minor effect on pH (changes pH by 0.15 to 0.23 units), suggesting that predicted pH without
43 consideration of organic water could be sufficient for the purposes of aqueous SOA chemistry. The mean
44 pH predicted in the Alabama forest (SOAS) was 0.94 ± 0.59 (median 0.93). ~~)-~~ pH diurnal trends followed
45 liquid water and were driven mainly by variability in RH; ~~in~~ during SOAS nighttime pH was near 1.5 ~~and~~
46 ~~during day,~~ while daytime pH was near 0.5. pH ranged from 0.5 to 2 in summer and 1 to 3 in the winter at
47 other sites. The systematically low pH levels ~~of predicted pH~~ in the southeast may have important
48 ramifications, such as significantly influencing acid-catalyzed reactions, gas-aerosol partitioning, and
49 mobilization of redox metals and minerals. Particle ion balances or molar ratios, often used to infer pH,

do not consider the dissociation state of individual ions or particle liquid water levels and so do not necessarily correlate with particle pH.

Keyword

Particle acidity, pH, particle water, LWC, f(RH), SOA, SOAS, SAS, SCAPE

1 Introduction

The concentration of the hydronium ion (H^+) in aqueous aerosols, or pH, is an important aerosol property that drives many processes related to particle composition and gas-aerosol partitioning (~~Jang et al., 2002; Meskhidze et al., 2003; Gao et al., 2004; Iinuma et al., 2004; Tolocka et al., 2004; Edney et al., 2005; Czoschke and Jang, 2006; Kleindienst et al., 2006; Surratt et al., 2007; Eddingsaas et al., 2010; Surratt et al., 2010~~)(Jang et al., 2002; Meskhidze et al., 2003; Gao et al., 2004; Iinuma et al., 2004; Tolocka et al., 2004; Edney et al., 2005; Czoschke and Jang, 2006; Kleindienst et al., 2006; Surratt et al., 2007; Eddingsaas et al., 2010; Surratt et al., 2010). ~~Despite its importance, measuring~~Measurement of pH is ~~not conserved during aerosol sampling because dilution makes its measurement~~highly challenging. ~~For this reason, and so~~ indirect proxies are often used to represent particle acidity. The most common is an ion balance; the charge balance of measurable cations and anions (excluding the hydronium ion). Although correlated with an acidic (net negative balance) or alkaline (net positive balance) aerosol (~~Surratt et al., 2007; Tanner et al., 2009; Pathak et al., 2011; Yin et al., 2014~~)(Surratt et al., 2007; Tanner et al., 2009; Pathak et al., 2011; Yin et al., 2014), an ion balance cannot be used as a ~~proxy for~~measure of the aerosol concentration of H^+ in air (i.e., moles H^+ per volume of air, denoted hereafter as H^+_{air}). This is due to two factors, first, an ion balance assumes all ions are completely dissociated, but multiple forms are possible, depending on pH (e.g., sulfate can be in the form of H_2SO_4 , HSO_4^- , or SO_4^{2-}). ~~A comparison between an ion balance predicted H^+_{air} to that from the full analysis discussed below, for this data set, is shown in the Supplementary material.~~Secondly, pH depends on the particle liquid water content (LWC) ~~(i.e., as pH is the concentration of H^+ in an aqueous solution), which.~~ LWC can vary considerably over the course of a day and between seasons ~~and influences~~significantly influencing pH (Seinfeld and Pandis, 2006)(Seinfeld and Pandis, 2006). Aerosol thermodynamic models, such as ISORROPIA-II (Nenes et al., 1998; Fountoukis and Nenes, 2007)(Nenes et al., 1998; Fountoukis and Nenes, 2007) and AIM (Clegg et al., 1998)(Clegg et al., 1998), are able to calculate LWC and particle pH, based on ~~measurements or model predictions~~concentrations of various aerosol species, temperature (T), and relative humidity (RH) and offer a more rigorous approach to obtain ~~the~~-aerosol pH (Pye et al., 2013)(Pye et al., 2013). ISORROPIA-

Particle water and Fine particle pH in the southeastern United States

81 II calculates the composition and phase state of an $\text{NH}_4\text{-SO}_4\text{-SO}_4^{2-}\text{-NO}_3\text{-Cl-Na-Ca-Ca}^{2+}\text{-K-Mg}^+\text{-}$
82 Mg^{2+} -water inorganic aerosol in thermodynamic equilibrium with water vapor and gas phase precursors.
83 The model has been tested with ambient data to predict acidic or basic compounds, such as $\text{NH}_{3(g)}$,
84 $\text{NH}_{4(p)}^+$, and $\text{NO}_{3(p)}^-$ (Meskhidze et al., 2003; Meskhidze et al., 2003; Nowak et al., 2006; Nowak et al., 2006;
85 Fountoukis et al., 2009; Fountoukis et al., 2009; Hennigan et al., 2014).

Field Code Changed

86 LWC is a function of RH, particle concentration and composition, and ~~predicted to be~~ is the most
87 abundant particle-phase species in the atmosphere, at least 2-3 times the total aerosol dry mass on a global
88 average (Pilinis et al., 1995; Liao and Seinfeld, 2005) (Pilinis et al., 1995; Liao and Seinfeld, 2005). At 90%
89 RH, the scattering cross-section of an ammonium sulfate particle can ~~be increased~~ increase by a factor of
90 five or more above that of the dry particle, due to large increases in size from ~~uptake of water (Malm,~~
91 ~~2001)~~ water uptake (Malm and Day, 2001). Because of this, LWC is the most important contributor to
92 direct radiative cooling by aerosols (Pilinis et al., 1995) (Pilinis et al., 1995), currently thought to be -0.45
93 Wm^{-2} (-0.95 Wm^{-2} to $+0.05 \text{ Wm}^{-2}$) (IPCC, 2013) (IPCC, 2013). LWC plays a large role in secondary
94 aerosol formation for inorganic and possibly organic species by providing a large aqueous surface for
95 increased gas uptake and a liquid phase where aqueous phase chemical reactions can result in products of
96 lower vapor pressures than the absorbed gases. (Ervens et al., 2011; Nguyen et al., 2013). In the eastern
97 US, it has been suggested that the potential for organic gases to partition to LWC is greater than the
98 potential to partition to particle-phase organic matter (Carlton and Turpin, 2013) (Carlton and Turpin,
99 2013), and partitioning of water soluble organic carbon (WSOC) into the particle phase becomes stronger
100 as RH (i.e., LWC) increases (Hennigan et al., 2008) (Hennigan et al., 2008). Thus LWC enhances particle
101 scattering effects directly by increasing particle cross sections (Nemesure et al., 1995) and indirectly by
102 promoting secondary aerosol formation (Nemesure et al., 1995) (Ervens et al., 2011; Nguyen et al., 2013).

103 The behavior of inorganic salts under variable RH is well established both experimentally and
104 theoretically. It is known that dry inorganic salts (or mixtures thereof) exhibit a phase change, called
105 deliquescence, when exposed to RH above a characteristic value. During deliquescence, the dry aerosol
106 spontaneously transforms (at least partially) into an aqueous solution (Tang, 1976; Wexler and Seinfeld,
107 1991; Tang and Munkelwitz, 1993) (Tang, 1976; Wexler and Seinfeld, 1991; Tang and Munkelwitz, 1993).

108 In contrast, due to its chemical complexity that evolves with atmospheric aging, the relationship of
109 organics to LWC is not well characterized, ~~and requires a parameterized approach. Despite the abundance~~
110 ~~and importance of LWC, it is not routinely measured. Thus, actual ambient particle total mass~~
111 ~~concentration is not well characterized. and requires a parameterized approach (Petters and Kreidenweis,~~
112 ~~2007). Relationships between volatility, oxidation level and hygroscopicity are not always straightforward~~
113 ~~and still remain to be fully understood (Frosch et al., 2011; Villani et al., 2013; Cerully et al., 2014;~~

114 [Hildebrandt Ruiz et al., 2014](#)). Despite the abundance and importance of LWC, it is not routinely
115 measured. Thus typically, particle total mass concentration (that includes liquid water) is often not
116 characterized. In general, LWC is measured by perturbing the in-situ RH. The loss of particle volume
117 when RH is lowered is assumed to be solely due to evaporated water. Approaches for LWC
118 measurements are classified into single particle size probes and bulk size quantification (~~Sorooshian et al.,~~
119 ~~2008~~)([Sorooshian et al., 2008](#)). Single size particle probes provide more information, i.e., size resolved
120 hygroscopic growth, and usually tend to be slow due to whole size range scanning. In contrast, bulk size
121 measurements quantify the total water amount directly. The LWC measurement presented in this paper by
122 nephelometers is a bulk measurement.

123 As part of the Southern Oxidant and Aerosol Study (SOAS), we made detailed measurements of particle
124 organic and inorganic composition (~~Xu et al., 2014~~), aerosol hygroscopicity ([Xu et al., 2015](#)), aerosol
125 hygroscopicity (~~Cerully et al., 2014~~)([Cerully et al., 2014](#)), and indirect measurements of particle LWC.
126 These data are used to first determine the particle water mass concentrations, which are then utilized in a
127 thermodynamic model for predicting pH. ~~This paper provides~~The fine particle LWC and pH data, ~~which~~
128 ~~from this analysis~~ are used in our other studies of secondary aerosol formation as part of SOAS ~~and~~
129 ~~discussed in companion papers to this work~~ (~~Cerully et al., 2014; Xu et al., 2014~~)([Cerully et al., 2014](#); [Xu](#)
130 [et al., 2015](#)). ~~In this analysis we use bulk properties and do not consider variability in parameters with~~
131 ~~particle size. Particle phase separations are also not considered, although they have been measured in bulk~~
132 ~~extracts of aerosols from the southeast (You et al., 2012). With ambient RHs typically higher than 60%,~~
133 ~~formation of non-crystalline organic coatings over an aqueous core are possible, but glassy states are not~~
134 ~~expected. Good agreement between measured particle water and ammonia partitioning to predictions~~
135 ~~using the bulk properties (discussed below) suggests these assumptions are reasonable.~~

2 ~~Date~~Data collection

2.1 Measurement sites

138 Aerosol measurements were conducted at the SEARCH ~~Centerville~~[Centreville](#) site (CTR; 32.90289 N,
139 87.24968 W, altitude: 126 m), located in Brent, Alabama, as part of ~~the~~-SOAS (Southern Oxidant and
140 Aerosol Study)-~~study~~ (<http://soas2013.rutgers.edu>). SOAS ground measurements were made from June 1st
141 to July 15th in the summer of 2013. CTR is a rural site within a large forested region dominated by
142 biogenic ~~VOCs emission~~[volatile organic compound \(VOC\) emissions](#), with minor local anthropogenic
143 emissions and some [plumes](#) transported ~~plumes (sulfur, CO~~from other locations ([coal-fired electrical](#)
144 [generating units, urban emissions](#), biomass burning, mineral dust). It is representative of background
145 conditions in [the](#) southeastern US and chosen to investigate biogenic secondary organic aerosol (SOA)

146 formation and its interaction with anthropogenic pollution [transported](#) from ~~long-range transport~~ [other](#)
147 [locations](#).

148 Additional measurements were also made at various sampling sites in and around the metropolitan
149 Atlanta region from May 2012 to December 2012 as part of a large health study: ~~the~~ [the](#) Southeastern Center
150 for Air Pollution and Epidemiology (SCAPE). A map of all ~~the~~ five sites is shown in Figure 1. The
151 [SCAPE](#) measurement sites include:

- 152 1) A road-side (RS) site (33.775602 N, 84.390957 W), situated within 5m from the interstate
153 highway (I75/85) in midtown Atlanta and chosen to capture fresh traffic emissions;
- 154 2) A near-road site (GIT site, 33.779125 N, 84.395797 W), located on the rooftop of the Ford
155 Environmental Science and Technology (EST) building at Georgia Institute of Technology (GIT),
156 Atlanta, roughly 30 to 40 m above ground level, 840 m from the RS site;
- 157 3) Jefferson Street (JST) (33.777501 N, 84.416667 W), a central SEARCH site representative of the
158 Atlanta urban environment, located approximately 2000 m west of the GIT site;
- 159 4) Yorkville (YRK) (33.928528 N, 85.045483 W), the rural SEARCH pair of JST, situated in an
160 agricultural region approximately 70 km west from the JST, GIT and RS sites.

161 More information on the SEARCH sites can be found ~~in~~ [elsewhere](#) (~~Hansen et al., 2003; Hansen et al.,~~
162 ~~2006~~) ([Hansen et al., 2003; Hansen et al., 2006](#)). We first focus on the SOAS campaign data, where ~~the~~
163 ~~widest~~ [wide](#) range of instrumentation was deployed (<http://soas2013.rutgers.edu>); ~~2~~ to develop a
164 comprehensive method of predicting LWC and pH_a as well as assessing their uncertainties. The approach
165 is then applied to the SCAPE site data to provide a broader spatial and temporal assessment of $\text{PM}_{2.5}$ -
166 ~~particle water and~~ pH in the southeastern US.

167 2.2 Instrumentation

168 [2.2a PILS-IC](#)

169 $\text{PM}_{2.5}$ or PM_1 (particles with aerodynamic diameters < 2.5 or $1.0 \mu\text{m}$ at ambient conditions) water soluble
170 ions were measured by a Particle-Into-Liquid-Sampler coupled ~~with~~ [to](#) an Ion Chromatograph (PILS-IC;
171 Metrohm 761 Compact IC). Similar setups are described in previous field studies (~~Orsini et al., 2003; Liu~~
172 ~~et al., 2012~~) ([Orsini et al., 2003; Liu et al., 2012](#)). Metrosep A Supp-5, 150/4.0 anion column and C 4,
173 150/4.0 cation column (Metrohm USA, Riverside, FL) were used to separate the PILS liquid sample
174 anions (sulfate, nitrate, chloride, oxalate, acetate, formate) and cations (ammonium, sodium, potassium,
175 calcium, magnesium) at a 20 min duty cycle. The PILS sample [ambient](#) air flow rate was $16.8 \pm 0.4 \text{ L}$
176 min^{-1} . URG (Chapel Hill, NC) cyclones were used to provide PM cut sizes of $\text{PM}_{2.5}$ for the 1st half of field

Particle water and Fine particle pH in the southeastern United States

177 study (June 1 to June 22) and PM₁ for the latter half (June 23 to July 15). Honeycomb acid (phosphoric
178 acid)- and base (sodium carbonate)-coated denuders removed interfering gases before entering the PILS.
179 The sample inlet was ~7 m above ground level and ~4 m long. The sampling line was insulated inside the
180 trailer (typical indoor T was 25 °C) and less than 1m in length to minimize possible changes in aerosol
181 composition prior to measurement. Periodic ~~1-hour~~hr blank measurements were made every day by
182 placing a HEPA filter (Pall ~~corp~~Corp.) on the cyclone inlet. All data were blank corrected. The PILS IC
183 was only deployed for the SOAS study.

184 2.2b AMS

185 A High-Resolution Time-of-Flight Aerosol Mass Spectrometer (HR-ToF-AMS, Aerodyne Research Inc.,
186 hereafter referred to as “AMS”) provided real time, quantitative measurements of the non-refractory
187 components of submicron aerosols (~~DeCarlo et al., 2006; Canagaratna et al., 2007~~)(DeCarlo et al., 2006;
188 Canagaratna et al., 2007). In brief, particles were first dried (RH < 20%) and then immediately sampled
189 through an aerodynamic lens into the high vacuum region of the mass spectrometer, then transmitted into
190 a detection chamber where particles impact on a hot surface (600 °C). Non-refractory species are flash
191 vaporized and then ionized ~~with~~by 70 eV electron impact ionization. The generated ions are extracted into
192 the time-of-flight mass spectrometer. Further details on the AMS setup and data processing can be found
193 in Xu et al. (~~2014~~2015).

194 2.2c CCNc

195 The particle hygroscopic parameter, κ (~~Petters and Kreidenweis, 2007~~)(Petters and Kreidenweis, 2007),
196 used to infer the hygroscopic properties (liquid water associated with organics), was obtained from size-
197 resolved CCN measurements ~~obtained with~~from a Droplet Measurement Technologies Continuous-Flow
198 Streamwise Thermal Gradient Cloud Condensation Nuclei counter (CFSTGC, referred to hereafter as
199 CCNc) (~~Roberts and Nenes, 2005; Lance et al., 2006~~)(Roberts and Nenes, 2005; Lance et al., 2006). The
200 CCNc exposes aerosols to a known supersaturation, then counts the activated particles that grow rapidly
201 to droplet size. Theory can be used to parameterize the water phase properties (here, expressed by κ ;
202 ~~Petters and Kreidenweis (2007)~~Petters and Kreidenweis (2007)) of the organic aerosol, based on the size
203 of particles that form CCN and their composition. A URG (Chapel Hill, NC) PM₁ cyclone was installed
204 for both AMS and CCNc. The details of the CCNc setup and data analysis procedure can be found in
205 ~~Cerully et al. (2014)~~Cerully et al. (2014).

Field Code Changed

Field Code Changed

2.2d Ambient vs Dry Nephelometers

PM_{2.5} (URG cyclones) aerosol light scattering coefficients (σ_{sp}) were measured online with two different nephelometers (Radiance Research M903) to infer LWC. Both were operated at nominally 3 L min⁻¹ controlled by critical orifices and vacuum pumps located some distance away from the instruments. Particle dry scattering was measured with a nephelometer located in the air-conditioned sampling trailer operated with a nafion dryer upstream, which that maintained an RH of 31.5 ± 1.9 % (study mean ± SD, n = 12,464 based on 5-min averages). The other was situated in a small white 3-sided wooden shelter (one side covered by a loose tarp) located a distance away from all building buildings to provide a scattering measurement at ambient T and RH. Both Both PM_{2.5} cut cyclones were located in ambient conditions, and both nephelometers were calibrated by CO₂ prior to the SOAS field campaign. Typical uncertainty is 3% for scattering coefficients (Mitchell et al., 2009) (Mitchell et al., 2009). In addition, the nephelometer RH sensors were calibrated by placing the sensors in a closed container above aqueous saturated salt solutions that had reached equilibrium (measurements made in a thermally insulated container after a period of a few hours). Solution temperatures were monitored. Details on the calibration results are provided in the Supplementary material. Material Section 1. Recorded RH was corrected by the resulting calibration results.

2.3 Determining LWC from nephelometers

Particle water was inferred from the ratio of wet ambient and dry PM_{2.5} (URG cyclones) scattering coefficients (σ_{sp}) measured by the two nephelometers (defined here as aerosol hygroscopic growth factor, $f(RH) = \sigma_{sp(wet)} \sigma_{sp(ambient)} / \sigma_{sp(dry)}$, where $\sigma_{sp(wet)}$, $\sigma_{sp(ambient)}$ and $\sigma_{sp(dry)}$ are particle scattering coefficients at ambient and dry RH conditions, respectively) following the method developed by other investigators (Carrico et al., 1998; Kotchenruther and Hobbs, 1998; Carrico et al., 2000; Malm, 2001; Sheridan et al., 2002; Magi and Hobbs, 2003; Kim et al., 2006) (Carrico et al., 1998; Kotchenruther and Hobbs, 1998; Carrico et al., 2000; Malm and Day, 2001; Sheridan et al., 2002; Magi and Hobbs, 2003; Kim et al., 2006). A difference between ambient and dry scattering coefficients is assumed to be caused solely by loss of water. Detailed derivations are provided in the Supplementary material. Material. $f(RH)$ is related to the measured particle scattering efficiencies (Q_s) and average particle diameter ($\overline{D_p}$) by;

$$\overline{D_{p,wet}} \overline{D_{p,ambient}} = \overline{D_{p,dry}} \sqrt{f(RH) Q_{s,wet} / Q_{s,dry}} \sqrt{f(RH) Q_{s,dry} / Q_{s,ambient}} \quad (1)$$

$Q_{s,wet}$, $Q_{s,ambient}$, $\overline{D_{p,wet}}$ are $\overline{D_{p,ambient}}$ are the average scattering efficiency and average particle diameter under ambient conditions, while $Q_{s,dry}$, $\overline{D_{p,dry}}$ represent the dry condition conditions. The method is based on the fact that for fine particles, particle light scattering is most effective by being mostly due to

Formatted: Space After: 0 pt

Formatted: Font: Bold, Italic

Formatted: Space Before: 6 pt, After: 6 pt

236 particles in the accumulation mode and can be related to scattering efficiencies and the diameter of
 237 average surface, for both ~~wet~~ambient and dry particle size distributions. Assuming that $\overline{Q_{wet}}/\overline{Q_{s,ambient}} =$
 238 $\overline{Q_{s,dry}}$ (see Supplementary Material Section 2 for justification and ~~Q_{wet} and Q_{dry} are of similar~~
 239 ~~magnitude; uncertainty analysis), it follows then that;~~

$$\overline{D_{p,wet}}\overline{D_{p,ambient}} = \overline{D_{p,dry}}\sqrt{f(RH)} \quad (2)$$

240 Since the LWC is equal to the difference between ~~wet~~ambient and dry particle volume, we get;

$$LWC = [f(RH)^{1.5} - 1]m/\rho_p = [f(RH)^{1.5} - 1]m_p\rho_w/\rho_p \quad (3)$$

241 ~~where m~~ Where m_p and ρ_p are dry particle mass and density, respectively; ρ_w is water density (constant
 242 1 g cm^{-3} is applied). For SOAS, dry PM_{2.5} mass concentrations were measured continuously by a TEOM
 243 (tapered element oscillating microbalance, 1400a, Thermo Fisher Scientific Inc., operated by
 244 Atmospheric Research & Analysis Inc.) were used., referred to hereafter as ARA). Particle density, ρ_p ,
 245 was computed from the particle composition, including AMS total organics, ammonium, and sulfate,
 246 which accounted for 90% of the measured PM_{2.5} (TEOM) dry mass (SOAS study mean). A typical
 247 organic density 1.4 g cm^{-3} is assumed (Turpin and Lim, 2001; King et al., 2007; Engelhart et al., 2008;
 248 Kuwata et al., 2012; Cerully et al., 2014)(Turpin and Lim, 2001; King et al., 2007; Engelhart et al., 2008;
 249 Kuwata et al., 2012; Cerully et al., 2014), and the density of ammonium sulfate is assumed to be 1.77 g
 250 cm^{-3} (Sloane et al., 1991; Stein et al., 1994)(Sloane et al., 1991; Stein et al., 1994). Particle density, ρ_p ,
 251 was calculated to be $1.49 \pm 0.04 \text{ g cm}^{-3}$ ($n = 4,393$) using mass fractions (ϵ):

$$\rho_p = \frac{1}{\epsilon(NH_4^+ + SO_4^{2-})/1.77 + \epsilon(Organics)/1.4} \frac{1}{\epsilon(NH_4^+ + SO_4^{2-})/1.77 + \epsilon(Organics)/1.4} \quad (\text{g cm}^{-3}) \quad (4)$$

252 The time-resolved composition data shows that dry particle density did not have a significant diurnal
 253 variability ($\pm 2.7\%$, SD/mean). (Note, SO_4 stands for sulfate in all its possible forms, from free to
 254 completely dissociated, the same applies to all other ions, e.g., NH_4^+ , NO_3^- , etc.), Supplementary Material
 255 Figure S2). In the following we refer to the particle water calculated by this method as $f(RH)$ _water. The
 256 uncertainty of $f(RH)$ _water is estimated to be 23% , mainly caused by $\overline{Q_{wet}}/\overline{Q_{dry}}$ ($\sim 20\%$), m (10%),
 257 $\sigma_{sp(wet)}$ (15% , mainly caused by the calculation of $\overline{Q_{s,ambient}}/\overline{Q_{s,dry}}$ (LWC error of 10% from assuming
 258 $\overline{Q_{s,ambient}}/\overline{Q_{s,dry}} = 1$, see Supplementary Material), m_p (10%), $\sigma_{sp(ambient)} / \sigma_{sp(dry)}$ (4.2%)
 259 (uncertainty for a single σ_{sp} measurement is 3% , Mitchell et al. (2009) Mitchell et al. (2009)), and ρ_p
 260 (2.7%), and ρ_p (2.7%). Note that LWC error depends on RH, and for SOAS average composition
 261 aerosol could increase to 21% for $RH > 90\%$ (Supplementary Material Figure S6).

3 Modeling Methods: Predicting LWC prediction and pH from aerosol composition

In most studies, such as SCAPE, particle water was not measured and must be determined based on aerosol composition. Both inorganic and organic components contribute to uptake of water vapor, establishing equilibrium for the ambient RH and T conditions. Thus, LWC is controlled by meteorological conditions and also by aerosol concentration and composition. Thermodynamic models, such as ISORROPIA-II, have been extensively used to predict LWC due to inorganic aerosol components (Fountoukis and Nenes, 2007)(Fountoukis and Nenes, 2007). Contributions to LWC by organic components are typically based on an aerosol hygroscopicity parameter, κ , which is determined by CCN data. Here we refer to particle water associated with inorganics and organics as W_i and W_o , respectively. Total particle water ($W_i + W_o$) is taken as the sum of water associated with individual aerosol chemical components (sum of ions and lumped organics) based on Zdanovskii-Stokes-Robinson (ZSR) relationship (Zdanovskii, 1936; Stokes and Robinson, 1966), with the assumption that the particles are internally mixed.

3.1 LWC from inorganic species

~~W_i was~~ Particle water associated with inorganic species (W_i) were predicted by ISORROPIA-II (Nenes et al., 1998; Fountoukis and Nenes, 2007)(Nenes et al., 1998; Fountoukis and Nenes, 2007). ISORROPIA-II calculates the composition and phase state of ~~an~~ a $K^+ - Ca^{2+} - Mg^{2+} - NH_4 - SO_4^{2-} - Na^+ - SO_4^{2-} - NO_3^- - Cl^- - Na - Ca - K - Mg^-$ -water inorganic aerosol in thermodynamic equilibrium with gas phase precursors. Chemical and meteorological data are necessary inputs. For our analysis at CTR, the inputs to ISORROPIA-II are the inorganic ions measured by the IC or AMS, RH measured by the outside ~~Nephelometer~~nephelometer, and temperature from the SEARCH site (ARA) meteorological data.

3.2 LWC from organic fraction

To determine the contributions to particle water by W_o , in SOAS the organic hygroscopicity parameter (κ_{org}) was ~~measured~~calculated based on the observed CCN activities of the organic fraction (Cerully et al., 2014)(Cerully et al., 2014) and in In the following analysis diurnal three-hour running averages are used in the calculation. (Diurnal plot is included in the Supplementary ~~material~~Material as Figure 5)S7). W_o is calculated using the following equation (Petters and Kreidenweis, 2007)(Petters and Kreidenweis, 2007).

$$W_o = \frac{m_s}{\rho_s} \frac{\kappa_{org}}{(1/RH - 1)} W_o = \frac{m_{org} \rho_w}{\rho_{org}} \frac{\kappa_{org}}{(1/RH - 1)} \quad (5)$$

Formatted: Font: Not Italic

290 where m_s is the organic mass concentration from AMS (Xu et al., 2014), and a typical organic density (ρ_s)
291 of 1.4 g cm^{-3} . Where m_{org} is the organic mass concentration from AMS (Xu et al., 2015), ρ_w is water
292 density, and a typical organic density (ρ_{org}) of 1.4 g cm^{-3} is used (Turpin and Lim, 2001; King et al.,
293 2007; Engelhart et al., 2008; Kuwata et al., 2012; Cerully et al., 2014) (Turpin and Lim, 2001; King et al.,
294 2007; Engelhart et al., 2008; Kuwata et al., 2012; Cerully et al., 2014).

295 3.3 pH prediction

296 The thermodynamic model, ISORROPIA-II (Fountoukis and Nenes, 2007) (Fountoukis and Nenes, 2007),
297 is used to predict particle pH, based on calculated ~~calculates the~~ equilibrium particle hydronium ion
298 concentration ~~in the aerosol~~ per volume air (H_{air}^+), which along with the LWC is then used to predict
299 particle pH. To correct for the LWC associated with the organic aerosol (not considered in ISORROPIA-
300 II), we recalculate pH by considering ~~the predicted particle hydronium ion concentration per volume air~~
301 ~~(H_{air}^+)~~ H_{air}^+ and total predicted water (W_i and W_o). The modeled concentrations are $\mu\text{g m}^{-3}$ air for H_{air}^+
302 and LWC. The pH is then,

$$pH = -\log_{10} H_{aq}^+ = -\log_{10} \frac{1000 H_{air}^+}{W_i + W_o} \quad (6)$$

303 ~~where~~ Where H_{aq}^+ (mol L^{-1}) is hydronium concentration in ~~aan~~ aqueous solution.

304 ISORROPIA-II has been tested in previous field campaigns where a suite of both gas and particle
305 components were measured (Nowak et al., 2006; Fountoukis et al., 2009) (Nowak et al., 2006; Fountoukis
306 et al., 2009). The model was able to predict the equilibrium partitioning of ammonia (Nowak et al.,
307 2006) (Nowak et al., 2006) in Atlanta and nitric acid (Fountoukis et al., 2009) (Fountoukis et al., 2009) in
308 Mexico City within measurement uncertainty. For instance, $\text{NH}_{3(g)}$, $\text{NH}_{4(p)}^+$, $\text{HNO}_{3(g)}$, and $\text{NO}_{3(p)}^-$ were
309 within 10%, 20%, 80%, and 20% of measurements (Fountoukis et al., 2009) (Fountoukis et al., 2009). In
310 this study, ISORROPIA-II was run in the “Forward mode” for metastable aerosol. Forward mode
311 calculates the equilibrium partitioning given the total concentration of various species (gas + particle)
312 together with RH and T as input. Reverse mode involves predicting the thermodynamic composition
313 based only on the aerosol composition. Here, we use the Forward mode with just aerosol phase data input
314 because it is less sensitive to measurement error than the Reverse mode (Hennigan et al., 2014) (Hennigan
315 et al., 2014). The W_i prediction ~~stays~~ remains the same (Reverse vs Forward: slope = 0.993, intercept = -
316 0.005, and $R^2 = 0.99$) no matter which approach is used. Gas phase input does have an important impact
317 on the H_{air}^+ calculation. ISORROPIA-II was tested with ammonia partitioning. ~~Discussed, which is~~
318 ~~discussed~~ in more detail below, ~~here~~. Here it is noted that we found that further constraining
319 ISORROPIA-II with measured $\text{NH}_{3(g)}$ (You et al., 2014) (You et al., 2014) resulted in a pH increase of 0.8

320 at CTR and that the predicted $\text{NH}_{3(\text{g})}$ matched the measured $\text{NH}_{3(\text{g})}$ well (slope = 1.07, intercept = -0.12 μg
321 m^{-3} , $R^2 = 0.76$). This also confirms that ISORROPIA-II predicts the pH in the ambient aerosol with
322 ~~good~~reasonable accuracy, as inputting the total (gas + aerosol) ammonium results in predictions that agree
323 with those observed. This is also in agreement with findings of ~~Hennigan et al. (2014)~~Hennigan et al.
324 (2014) and ~~Fountoukis et al. (2009)~~Fountoukis et al. (2009), both of whom found that ISORROPIA-II
325 reproduced the partitioning of ammonia and inorganic nitrate in Mexico City during the MILARGO
326 campaign.

327 3.4 Assumptions

328 In the following analysis we use bulk properties and do not consider variability in parameters with
329 particle size. Particulate organic and inorganic species are assumed to be internally mixed in the liquid
330 phase due to the high RH ($73.8 \pm 16.1\%$) typical of this study and because a large fraction of the ambient
331 aerosol organic component is from isoprene SOA (Xu et al., 2015), which are liquids at $\text{RH} \geq 60\%$ (Song
332 et al., 2015). Particle liquid phase separations are not considered, although they have been measured in
333 bulk extracts of aerosols from the southeast (You et al., 2012). It is reported that liquid-liquid phase
334 separation can occur when the O:C ratio of the organic material is ≤ 0.5 . More experiments showed that it
335 is possible to have phase separation for $\text{O:C} < 0.7$, but not for $\text{O:C} \geq 0.8$ (Bertram et al., 2011; Song et al.,
336 2012; You et al., 2013). SOAS average $\text{O:C} = 0.75 (\pm 0.12)$ is in the transition between these two regimes.
337 According to Figure 2 in Bertram et al. (2011), at RH typically $> 60\%$ and organic:sulfate mass ratio > 1 ,
338 it is not possible to have phase separation, which is the case for our sampling sites. Based on our basic
339 assumption of no liquid-liquid phase separation, pH is considered to be homogeneous in a single particle.
340 However, separated phases would likely have different pHs if liquid-liquid phase separation occurs. In
341 that case, pH should be calculated based on the amounts of water and H_{air}^+ in each phase. Gas-particle
342 phase partitioning will change according, due to these separated phases. There are models that are set up
343 to calculate these thermodynamics (e.g., AIOMFAC), but none is yet able to address the compositional
344 complexity of ambient SOA. (Zuend et al., 2010; Zuend and Seinfeld, 2012) Although it is often true that
345 non-ideal interactions between organic and inorganic species exist, good agreement between measured
346 particle water and ammonia partitioning to predictions using the bulk properties (discussed below)
347 suggests these assumptions are reasonable.

348 **4 Results**

349 **4.1 Summary** Overall summary of meteorology and PM composition at SOAS and SCAPE sites

350 For the SOAS study period, mean T and RH were 24.7 ± 3.3 °C and 73.8 ± 16.1 % (mean \pm SD),
351 respectively. This resulted in a $f(RH)$ water level of 4.52 ± 3.75 $\mu\text{g m}^{-3}$, with a maximum value of 28.41
352 $\mu\text{g m}^{-3}$. In comparison, SOAS mean dry $\text{PM}_{2.5}$ mass was 7.72 ± 4.61 $\mu\text{g m}^{-3}$, implying that the fine
353 aerosols were roughly composed of 37% water, on average. Mean T and RH for SCAPE sites are listed in
354 Table 3. Summer T means were all above 21 °C, including CTR. RH means were all high (> 60%) for
355 summer and winter, which is typical for the southeastern US.

356 Of the sites in the southeastern US discussed in this paper, CTR was the least influenced by
357 anthropogenic emissions having the lowest black carbon (BC) concentrations (measured by a MAAP,
358 Thermo Scientific, model 5012). At CTR, the mean BC = 0.26 ± 0.21 $\mu\text{g m}^{-3}$ (\pm SD), whereas mean BC
359 concentrations at the other rural site (YRK) was 0.36 $\mu\text{g m}^{-3}$. The representative Atlanta site (JST) BC
360 was on average 0.71 $\mu\text{g m}^{-3}$, and higher for sites closer to roadways, 0.96 $\mu\text{g m}^{-3}$ (GIT) and 1.96 $\mu\text{g m}^{-3}$
361 (RS).

362 ~~For the SOAS study period, mean T and RH were 24.7 ± 3.3 °C, 73.8 ± 16.1 % (mean \pm SD), respectively.~~
363 ~~This resulted in $f(RH)$ water level of 4.52 ± 3.75 $\mu\text{g m}^{-3}$, with a maximum value of 28.41 $\mu\text{g m}^{-3}$. In~~
364 ~~comparison, SOAS mean dry $\text{PM}_{2.5}$ mass was 7.72 ± 4.61 $\mu\text{g m}^{-3}$, implying that the fine aerosols were~~
365 ~~composed of roughly 37% water on average. Mean T and RH for SCAPE sites are listed in Table 3.~~
366 ~~Summer T means were all above 21 °C, including CTR. RH means were all high (> 60%) for summer and~~
367 ~~winter, which is typical for the southeastern US.~~

368 A more comprehensive suite of ions will provide a better prediction of W_i . However, in the southeastern
369 US, inorganic ions are currently dominated by sulfate and ammonium. During SOAS, the PILS-IC
370 provided a more comprehensive and accurate measurement of water-soluble ions than AMS, which
371 measured only non-refractory sulfate, ammonium, nitrate, and chloride. Refractory, but water soluble ions,
372 such as sodium and associated chloride, and crustal elements including calcium, potassium, and
373 magnesium were present in PM_1 , but in very low concentrations. Contributions of these ions are more
374 important in $\text{PM}_{2.5}$ than for PM_1 , which tend to reduce aerosol acidity. For instance, Na^+ has a
375 significantly higher mean in $\text{PM}_{2.5}$ at 0.056 $\mu\text{g m}^{-3}$ (1st half of SOAS study) than 0.001 $\mu\text{g m}^{-3}$ in PM_1 (2nd
376 half of SOAS study) ~~at CTR.~~ Four, one day-long, dust events (06/12, 06/13, 06/16, and 06/21) in the
377 SOAS data set have been excluded from this analysis as assumptions relating to internal mixing of $\text{PM}_{2.5}$

378 components are less valid in these cases. Excluding these days, the mean Na⁺ in PM_{2.5} drops to 0.024 μg
379 m⁻³.

380 If the fraction of the refractory ions (e.g., Na, ~~Ca~~⁺, K, ~~Mg~~⁺, Ca²⁺, Mg²⁺) is negligible compared to the
381 SO₄, ~~NH₄~~ (Note, SO₄ stands for sulfate in all its possible forms, from free to completely dissociated),
382 NH₄[±], and NO₃⁻, the AMS data sufficiently constrains particle composition for thermodynamic
383 calculations; this apparently is the case for most of the time in the southeast (Supplementary
384 ~~material~~ Material Section 54). For PM₁ SO₄ and NH₄[±], AMS and PILS-IC were in good agreement
385 (sulfate SO₄ slopes within 20 %, R² = 0.90; ammonium NH₄[±] within 1%, R² = 0.81). Similar agreement
386 was also found for AMS PM₁ SO₄ and NH₄[±] versus PILS-IC PM_{2.5} SO₄ and NH₄[±] (see⁺. (See Figure 2 for
387 comparison of complete data set). These data indicate little SO₄ and NH₄[±] between the 1.0 and 2.5 μm
388 size range (PM_{2.5} – PM₁). Because of the agreement between these dominant ions, ISORROPIA-II-
389 predicted W_i for all ions measured with the PILS-IC throughout the study (includes both PM₁ and PM_{2.5})
390 agreed with W_i based on AMS inorganic species (i.e., only ammonium and sulfate) having an orthogonal
391 slope of 1.18, Figure 2c.

392 4.2 Results from the SOAS Centreville site

393 4.2a LWC, pH and ion balances at Centreville

394 The diurnal variation of LWC contributed by W_i and W_o , along with total measured water, ambient T, RH,
395 and solar radiation at CTR is shown in Figure 3. Predicted and measured LWC trends were in good
396 overall agreement, although the largest discrepancy was observed during the daytime when the LWC
397 level was low and more difficult to measure and accurately predict. Nighttime RH median values were
398 between 85% and 90% and resulted in significant water uptake that reached a peak just after sunrise near
399 7:30 am (local time). The dramatic peak in LWC starting at roughly 5:00 am, reaching a maximum
400 between 7:30 and 8:00 am is likely due to RH increasing above 90%, at which point uptake of water
401 rapidly increases with increasing RH. The similar rapid hygroscopic growth before sunrise was also
402 observed at GIT, RS, and JST (Nov) (Figure 11). After sunrise, rising temperatures led to a rapid drop in
403 RH, resulting in rapid loss of particle water. LWC reached lowest levels in the afternoon ~2 μg m⁻³, only
404 20% of the peak value. W_o varied more than W_i diurnally; W_o max/min ratio was 13.1 compared to 4.1 for
405 W_i .

406 At CTR, the aerosol was highly acidic, with predicted mean pH = 0.94 ± 0.59 (±SD). The minimum and
407 maximum pH were -0.94 and 2.23 respectively, and pH varied by approximately 1 on average throughout
408 the day (Figure 4a). That is, the H_{air}^+ /LWC ratio increased by a factor of 10 from night to day. LWC

409 max/min ratio was 5, whereas H_{air}^+ diurnal variation was significantly less (Figure 4b), indicating that the
410 diurnal pattern in pH was mainly driven by particle water dilution. This is further demonstrated in Figure
411 4d, which shows the diurnal variation in the NH_4^+/SO_4^{2-} molar ratio (the main ions driving pH), with only
412 slightly lower ratios during the day. The study mean (\pm SD) NH_4^+/SO_4^{2-} molar ratio was 1.4 (\pm 0.5). As
413 LWC is mainly controlled by RH and temperature, the pH diurnal variation was thus largely driven by
414 meteorological conditions, not aerosol composition.

415 In part, because of the diurnal variation of LWC, a simple ion balance or NH_4^+/SO_4^{2-} molar ratio or per
416 volume air concentration of aerosol hydronium ion (H_{air}^+) alone cannot be used as a proxy for pH in the
417 particle. Figure 5a shows a weak inverse correlation ($R^2 = 0.36$) between ion balance and pH. An ion
418 balance of an aerosol is usually calculated as follows (in unit of nmol equivalence m^{-3}), for a $NH_4^+-Na^+-$
419 $SO_4^{2-}-NO_3^- -Cl^-$ -water inorganic aerosol.

$$Ion\ Balance = \frac{[SO_4^{2-}]}{48} + \frac{[NO_3^-]}{62} + \frac{[Cl^-]}{35.5} - \frac{[NH_4^+]}{18} - \frac{[Na^+]}{23} \quad (7)$$

420 Where $[SO_4^{2-}]$, $[NO_3^-]$, $[Cl^-]$, $[NH_4^+]$, and $[Na^+]$ are concentrations of these ions in units of $g\ m^{-3}$. An ion
421 balance is also a bad indicator of pH because it poorly predicts the aerosol concentration of H_{air}^+ . An ion
422 balance assumes all ions are completely dissociated, but multiple forms are possible, depending on pH
423 (e.g., sulfate can be in the form of H_2SO_4 , HSO_4^- , or SO_4^{2-}). For example, if aerosol sulfate remains in the
424 free form of H_2SO_4 , it doesn't add protons. Thus, an ion balance usually overestimates protons and is only
425 moderately correlated with H_{air}^+ (Figure 5b).

426 ***LWC uncertainty:***

427 In estimating the water uncertainty, we consider W_i and W_o separately. The uncertainty of W_i is estimated
428 by propagating the measurement uncertainty of ions and RH through the ISORROPIA-II thermodynamic
429 model by finite perturbations about the model base state. Uncertainties of ions were estimated by
430 difference between IC-ions and AMS-ions, as well as PILS-IC measurement uncertainty (Table 2). Na^+ is
431 excluded because it is not measured by the AMS. PILS-IC instrumental uncertainty is estimated to be 15%
432 from the variability in standards (variability is calibration slopes), blanks, sample airflow rate, and liquid
433 flow rate (one ~~standard deviation~~, SD). The total ion uncertainties are listed in Table 2. SO_4 has a higher
434 uncertainty, at 25%, than the rest, which are at 15%. These combined uncertainties lead to an W_i
435 uncertainty of 25% (Figure 3), ~~which is the same as the SO_4 uncertainty, since as the most hygroscopic~~
436 ~~ion it controls W_i uptake. Although the AMS data set does not include Na and crustal elements, it is still~~
437 ~~generally capable of predicting W_i as it measures the most hygroscopic and abundant ions SO_4 , NH_4 , and~~

Formatted: Heading 3

438 ~~NO₃ (Figure 2).6), which is the same as the SO₄ uncertainty. SO₄, one of the most hygroscopic ions~~
 439 ~~(Petters and Kreidenweis, 2007), controls W_i uptake.~~

440 For the SOAS study, the RH probe in the ambient nephelometer (Humitter 50U, VAISALA Inc.) has a
 441 stated ~~maximum~~ uncertainty of 5% at RH = 90%. RH biases with respect to environment conditions
 442 can also occur due to placement of the probe. Based on RH comparisons between ARA, Rutgers (~~Nguyen~~
 443 ~~et al., 2014~~)([Nguyen et al., 2014](#)), and the Georgia Tech instrumentation, a systematic bias as large as 10%
 444 is found. Given this, we consider an RH probe factory uncertainty (5%) as a typical value and inter-
 445 comparison difference (10%) as an extreme condition. In this analysis, RH was adjusted by ±5% and ±10%
 446 and W_i recalculated (Figure 47). A ±5% perturbation in RH leads to a 91% (slope - 1, see Figure 7) error
 447 for 5% perturbation above the measured value (1.05RH) and 29% error for a perturbation below the
 448 measured value (0.95RH). We take 60% as average uncertainty. Higher uncertainty is introduced with
 449 increasing RH, owing to the exponential growth of LWC with RH and results in the asymmetric LWC
 450 uncertainty. Combining W_i uncertainty from ions (25%) and RH (60%), the overall uncertainty is
 451 calculated as 65%.

452 The uncertainty sources for W_o are ~~κ, ρ_s, m_s, and RH (Equation 5). The uncertainties of these parameters~~
 453 ~~are estimated to be 20% (Cerully et al., 2014), 10%, 20%, and 5% (from above), respectively. In summary,~~
 454 ~~the overall uncertainty of W_o is 30%.~~
 455 ~~κ, ρ_s, m_s, and RH (Equation 5). The uncertainties of these~~
 456 ~~parameters are estimated to be 26% (details can be found in Supplementary Material Section 3), 10%,~~
 457 ~~20%, and 5% (from above), respectively. In summary, the overall uncertainty of W_o is 35%.~~

457 The total uncertainty of LWC can be expressed as a sum of W_i and W_o uncertainties, where ε_iε_i is the
 458 mass fraction. ε_{W_o} was found to be 36% and ε_{W_i} was 64%.

$$\frac{\delta_{LWC}}{LWC} = \sqrt{\left(\frac{\delta_{W_i}}{W_i}\right)^2 + \left(\frac{\delta_{W_o}}{W_o}\right)^2} \frac{\delta_{LWC}}{LWC} = \sqrt{\left(\varepsilon_{W_i} \frac{\delta_{W_i}}{W_i}\right)^2 + \left(\varepsilon_{W_o} \frac{\delta_{W_o}}{W_o}\right)^2} \quad (7)(8)$$

459 Given the above, $\frac{\delta_{LWC}}{LWC}$ is 43%. This method of assessing predicted LWC uncertainty can be applied to
 460 SCAPE sites as well. The specific predicted LWC at SCAPE sites were calculated and are listed in Table
 461 3. W_i uncertainty associated with ions is the same as noted above, 25%, because it is estimated by PILS-
 462 IC and AMS differences. Similar uncertainties in W_i at the SCAPE sites are expected if RH uncertainties
 463 are similar at all sites.

464 **4.3 pH uncertainty:**

Formatted: Heading 3

465 As pH is based on H_{air}^+ and LWC, the uncertainty of pH can be estimated from these two parameters. We
 466 applied the adjoint model of ISORROPIA, ANISORROPIA (Capps et al., 2012)(Capps et al., 2012), to
 467 quantify the sensitivity of predicted $H^{\pm}H_{air}^+$ to the input aerosol species at the conditions of the
 468 thermodynamic calculations. pH uncertainty ~~resulted~~resulting from aerosol composition is then
 469 determined by propagating the input parameter uncertainties, using ANISORROPIA sensitivities, to the
 470 corresponding $H^{\pm}H_{air}^+$ and pH uncertainty.

Formatted: Font: Not Bold

471 We now assess how pH of PM_{2.5} is affected by using an incomplete measurement of ionic species by
 472 comparing the pH predicted based on the more complete suite of ions measured by the PILS-IC versus the
 473 AMS, during SOAS. Sensitivities of aerosol species to $H^{\pm}H_{air}^+$ were calculated by ANISORROPIA with
 474 PILS-IC data and presented as partial derivatives (Table 2). Higher sensitivity values imply the inorganic
 475 ion is more important for ion balance. In the SOAS study, $H^{\pm}H_{air}^+$ is most sensitive to SO₄, and then
 476 NH₄⁺, as they were the major ions. Uncertainties of ions were estimated by the difference between IC-
 477 ions and AMS-ions, as well as PILS-IC measurement uncertainty. Since Na⁺ is not measured by AMS, we
 478 cannot estimate the difference between PILS-IC and AMS. The loadings and sensitivities of NO₃⁻ and Cl⁻
 479 were very low, so they are assumed not to contribute much to $\frac{\delta_{H^{\pm}}}{H^{\pm}} \frac{\delta_{H_{air}^+}}{H_{air}^+}$. Given this, $\frac{\delta_{H^{\pm}}}{H^{\pm}} \frac{\delta_{H_{air}^+}}{H_{air}^+}$ is determined
 480 by;

$$\begin{aligned} \frac{\delta_{H^{\pm}}}{H^{\pm}} &= \sqrt{\left(\frac{\partial H^{\pm}}{\partial SO_4} \frac{\delta_{SO_4}}{SO_4}\right)^2 + \left(\frac{\partial H^{\pm}}{\partial NH_4} \frac{\delta_{NH_4}}{NH_4}\right)^2 + \left(\frac{\partial H^{\pm}}{\partial Na} \frac{\delta_{Na}}{Na}\right)^2} \frac{\delta_{H_{air}^+}}{H_{air}^+} \\ &= \sqrt{\left(\frac{\partial H_{air}^+}{\partial SO_4} \frac{\delta_{SO_4}}{SO_4}\right)^2 + \left(\frac{\partial H_{air}^+}{\partial NH_4} \frac{\delta_{NH_4}}{NH_4}\right)^2 + \left(\frac{\partial H_{air}^+}{\partial Na} \frac{\delta_{Na}}{Na}\right)^2} \end{aligned} \quad (8)(9)$$

481 Based on the input for Equation 89 (Table 2), $\frac{\delta_{H^{\pm}}}{H^{\pm}} \frac{\delta_{H_{air}^+}}{H_{air}^+}$ is estimated as 14%. LWC is most sensitive to RH
 482 fluctuations, so it is considered the main driver of LWC uncertainty in the pH calculation. As discussed,
 483 we artificially adjusted RH by $\pm 5\%$ and $\pm 10\%$ (10% is considered an extreme condition). $H^{\pm}H_{air}^+$, W_i , W_o ,
 484 as well as pH were all recalculated using 90%, 95%, 105%, and 110% of the actual measured RH. RH+5%
 485 and RH-5% lead to 12% and 6% variation in pH based on orthogonal regression slopes, respectively
 486 (Figure 58). RH-10% results in only 10% variation, however, RH+10% results in a 45% variation, and the
 487 coefficient of determination (R^2) between pH calculated based on RH+10% and original RH drops to only
 488 0.78, while for all other cases $R^2 > 0.96$. The disproportionately large effect of the positive uncertainty is
 489 caused by the exponential increase of LWC with RH, as RH reaches high levels (>90%). Assuming the

490 stated manufacturer uncertainty (5%) for our RH uncertainty, pH uncertainty is estimated to be 6%-12%.

491 We take 12% as $\frac{\partial pH}{\partial LWC} \delta_{LWC}$ for further calculations.

492 SO_4 was found to contribute the most to $\frac{\delta_{H^\pm}}{H^\pm} \frac{\delta_{H_{air}^+}}{H_{air}^+}$, NH_4^\pm and Na^\pm followed. SO_4 and NH_4^\pm are the two
 493 most abundant inorganic components in aerosols and controlling aerosol acidity. Finally, the total pH
 494 uncertainty is the combination of LWC and the uncertainty associated with $H^\pm H_{air}^+$, which is computed
 495 from the definition of pH (Equation 6).

$$\frac{\delta_{pH}}{pH} = \sqrt{\left(\frac{\partial pH}{\partial H^\pm} \delta_{H^\pm}\right)^2 + \left(\frac{\partial pH}{\partial LWC} \delta_{LWC}\right)^2} \frac{\delta_{pH}}{pH} = \sqrt{\left(\frac{\partial pH}{\partial H_{air}^+} \delta_{H_{air}^+}\right)^2 + \left(\frac{\partial pH}{\partial LWC} \delta_{LWC}\right)^2} \quad (9)(10)$$

496 where $\frac{\partial pH}{\partial H^\pm} \frac{\partial pH}{\partial H_{air}^+}$ can be derived from Equation (6) as

$$\frac{\partial pH}{\partial H^\pm} \frac{\partial pH}{\partial H_{air}^+} = -\frac{1}{2.303} \frac{1}{\frac{H^\pm}{LWC}} \frac{1}{\frac{H_{air}^+}{LWC}} = -\frac{1}{2.303} \frac{1}{H^\pm} \frac{1}{H_{air}^+} \quad (10)(11)$$

497 From Equation 9 and the uncertainties of $H^\pm H_{air}^+$ and LWC (Equation 7 and 8), we estimate the pH
 498 uncertainty for the SOAS dataset to be 13% (based on the specific uncertainties considering here). pH

499 uncertainties at SCAPE sites were also assessed via this method. As discussed above, $\frac{\delta_{H^\pm}}{H^\pm} \frac{\delta_{H_{air}^+}}{H_{air}^+}$ was found
 500 to be 14% for the SOAS study, due to IC and AMS data set differences and PILS-IC instrumental
 501 uncertainty. This same uncertainty is applied to SCAPE, where no PILS-IC data were available. Because
 502 aerosol ~~compositions~~ composition at all sites are similar, based on filter IC analysis (Supplementary
 503 ~~material~~ Material Figure 6S8), similar sensitivities of $H^\pm H_{air}^+$ to ions are expected. However, actual
 504 uncertainty for each sampling period is possibly higher due to higher loadings of refractory ions at
 505 SCAPE sites due to contributions from urban emissions. Refractory ions not measured by the AMS (i.e.
 506 Na^\pm , K , Ca , Mg , Ca^{2+} , Mg^{2+}), have a minor effect on predicting LWC, but may have an
 507 important effect on pH (e.g., result in higher pH) in locations (e.g., pH higher) where they could
 508 substantially contribute to the overall ion balance.

509 ~~pH uncertainty in different seasons:~~ 4.2b Model validation: Prediction of liquid water

510 Several LWC measurements were made at CTR during SOAS. In addition to $f(RH)$ water (4.52 ± 3.75
 511 $\mu\text{g m}^{-3}$), particle water was quantified with a Semi-volatile Differential Mobility Analyzer (SVDMA).
 512 With this method, a SOAS study mean particle water concentration of $4.27 \pm 3.69 \mu\text{g m}^{-3}$ (\pm STD) was
 513 obtained (Nguyen et al., 2014). The orthogonal regression between these two measurements (SVDMA
 514 water vs $f(RH)$ water) has slope = 0.91, intercept = -0.03, $R^2 = 0.35$. Differences could be caused by

515 differences in size-resolved composition (particle composition beyond PM_{10} that contributes LWC;
516 SVDMA scans up to 1.1 μm , while $f(RH)$ water is based on $PM_{2.5}$), instrument sample heating (i.e., the
517 degree to which the instrument was close to ambient conditions, especially when ambient RH was high,
518 and most sensitive to slight T differences), and differences in RH probe calibrations.

519 CTR predicted total LWC, $(W_i + W_o)$, was $5.09 \pm 3.76 \mu\text{g m}^{-3}$ and agreed well with $f(RH)$ water. The
520 total predicted water was highly correlated and on average within 10% of the measured water, with slope
521 = 0.91, intercept = 0.46, $R^2 = 0.75$ (see Figure 9). Since excluding refractory ions (Section 4.1) and not
522 considering gas phase species in the ISORROPIA-II calculations do not significantly affect the LWC
523 prediction, its comparison across sites is less uncertain than pH.

524 4.2c Model validation: Prediction of pH

525 ISORROPIA-II calculations of pH at CTR for the SOAS study were evaluated by comparing measured
526 and predicted $\text{NH}_{3(g)}$. Although NH_4^+ and $\text{NH}_{3(g)}$, along with other aerosol components, are input into the
527 model, comparing ambient NH_4^+ and $\text{NH}_{3(g)}$ to model predictions is not a circular analyses. For each
528 observed data point, the model calculates total ammonia from the NH_4^+ and $\text{NH}_{3(g)}$ input, and then
529 calculates the gas-particle ammonia partitioning assuming equilibrium. There are also other various
530 assumptions/limitations associated with the model. Figure 10 shows the SOAS study time series of
531 measured and predicted $\text{NH}_{3(g)}$ and the fraction of ammonia in the gas phase $(\text{NH}_{3(g)} / (\text{NH}_{3(g)} + \text{NH}_4^+))$.
532 Measured and predicted $\text{NH}_{3(g)}$ are in good agreement. Periods when almost all ammonia was in the gas
533 phase (ratio near 1) are related to precipitation events (06/10, 06/24, 06/28, 07/03, 07/04) when aerosol
534 concentrations were very low. Not including these events, the study mean (\pm SD) fraction ammonia in the
535 gas phase was 0.41 (\pm 0.16) (median value is also 0.41). These results provide confidence in
536 ISORROPIA-II calculations of particle pH, and demonstrate the utility of including both measurements of
537 particle and gas phases in these types of studies.

538 When gas and particle data are not available, pH predictions are not as accurate (Hennigan et al., 2014).
539 Running ISORROPIA-II in the forward mode, but with only aerosol concentrations as input, may result in
540 a bias in predicted pH due to repartitioning of ammonia in the model. In the southeast, where pH is
541 largely driven by SO_4 and NH_4^+ , the aerosol NH_4^+ input will be partitioned in the model between gas and
542 particle phases to establish equilibrium. Sulfate repartitioning does not occur since it is non-volatile.
543 Thus, NH_4^+ will be lost from the particle and a lower pH predicted. At CTR ammonia partitioning has
544 been included in all model runs, but as no $\text{NH}_{3(g)}$ was available for SCAPE. Assuming the average
545 $\text{NH}_{3(g)}/\text{NH}_4^+$ ratio from CTR applies to all SCAPE sites to estimate $\text{NH}_{3(g)}$, along with measured particle
546 composition at each site, we got pH increases ranging from 0.87 to 1.38. In the following, all pHs

547 reported for SCAPE are corrected for this bias (i.e., pHs are increased by 1 to simplify the correction).
548 Note that ammonia partitioning does not significantly affect the LWC prediction (W_i predicted without
549 $\text{NH}_{3(g)}$ vs W_i predicted with $\text{NH}_{3(g)}$: slope = 1.00, intercept = -0.01 $\mu\text{g m}^{-3}$, $R^2 = 0.98$).

550 4.3 LWC and pH at other sites in the southeast (SCAPE sites)

551 4.3a Seasonal trends

552 The methods developed and verified at CTR are now applied to the SCAPE study where fewer species
553 was measured. LWC predictions at all SCAPE sites are shown in Table 3, providing insights on seasonal
554 trends of LWC in the southeast. The overall summer LWC mean was 5.02 $\mu\text{g m}^{-3}$ and winter mean 2.22
555 $\mu\text{g m}^{-3}$.

556 At the SCAPE sites, JST, YRK, GIT, and RS, summer mean pHs were between 1 and 1.3, similar to CTR
557 (mean of 0.94). In winter the pHs (mean between 1.8 and 2.2) were higher by ~ 1 unit. Although LWC
558 was higher in summer, which tends to dilute H_{air}^+ and increase pH, summer pH was lower due to higher
559 ion (i.e., sulfate) concentrations (Table 3). Similar diurnal pH patterns were seen at all sites in all seasons
560 and follow the diurnal variations of particle water (Figure 11). Overall the pH in the southeast is very low,
561 between 1 and 2 (mean), in both rural and urban environments. pH values in summer at various sites were
562 similar (1 to 1.3), suggesting a fairly homogeneous distribution of acidity due to spatially uniform sulfate
563 in the southeastern US (Zhang et al., 2012). In winter the diurnal range in pH was roughly 2 units, while
564 the diurnal range in summer was smaller, with pH varying by roughly 1.

565 Recall at CTR, 10% RH uncertainty can result in a pH prediction error of up to 45% due to the high RHs
566 observed during the study. We estimated pH uncertainty from W_i and W_o by + 10% RH for each SCAPE
567 site. As Table 3 shows, the pH uncertainty associated with RH is much lower in winter (only 1-3%) than
568 summer (20-40%), although RH averages were similar, e.g., JST in May ($67 \pm 19\%$) and Nov ($63 \pm 19\%$),
569 with even higher RH in winter at YRK. Total pH uncertainty at all SCAPE sites are calculated by the
570 same method as CTR. Table 3 shows that higher RH and T result in larger pH uncertainty. In summer, pH
571 uncertainty is mainly caused by RH; while in winter, it can be attributed mostly to uncertainty in ion
572 concentrations. ~~pH predicted for the SCAPE sites likely has a systematic bias of roughly -1 because $\text{NH}_{3(g)}$~~
573 ~~is not included in the ISORROPIA-II calculation (recall including $\text{NH}_{3(g)}$ increased the CTR pH by 0.8).~~
574 ~~At JST, YRK, GIT, and RS sites, summer mean pH were between 0 and 0.3. Adding 1 pH unit of~~
575 ~~systematic bias makes pH at these southeastern sites between 1 and 1.3, which is consistent with the CTR~~
576 ~~pH of 0.94 ± 0.59 (\pm SD). $\text{NH}_{3(g)}$ does not significantly affect the LWC prediction (W_i predicted without~~
577 ~~$\text{NH}_{3(g)}$ vs W_i predicted with $\text{NH}_{3(g)}$: slope = 1.00, intercept = -0.01 $\mu\text{g m}^{-3}$, $R^2 = 0.98$).~~

4.4 LWC comparison to predictions and seasonal and diurnal trends in the southeast

4.3b The role of W_o

Several LWC measurements were made at CTR during SOAS. In addition to $f(RH)$ -water ($4.52 \pm 3.75 \mu\text{g m}^{-3}$), particle water was quantified with a Semi-volatile Differential Mobility Analyzer (SVDMA). With this method, a SOAS study mean particle water concentration of $4.27 \pm 3.69 \mu\text{g m}^{-3}$ (\pm SD) was obtained (Nguyen et al., 2014). The orthogonal regression between these two measurements (SVDMA water vs $f(RH)$ -water) has slope = 0.91, intercept = -0.03, $r = 0.59$. Differences could be caused by differences in size-resolved composition (particle composition beyond PM_{10} that contributes LWC; SVDMA scans up to 1.1 μm , while $f(RH)$ -water is based on $\text{PM}_{2.5}$), instrument sample heating (i.e., the degree to which the instrument was close to ambient conditions, especially when ambient RH was high, hence most sensitive to slight T differences), and differences in RH probe calibrations.

The particle water predicted from the sum of W_i and W_o agreed well with $f(RH)$ -water. That is, the total predicted water was highly correlated and on average within 10% of the measured water, with slope = 0.91, intercept = 0.46, $r = 0.87$ (see Figure 6).

Since excluding refractory ions (Section 4.1) and not considering gas phase species in the ISORROPIA-II calculations do not significantly affect the LWC prediction, its comparison across sites is less uncertain than pH. CTR total LWC is predicted to be $5.09 \pm 3.76 \mu\text{g m}^{-3}$. LWC predictions at all the other sites are shown in Table 3, providing insights on seasonal trends of LWC in the southeast. The overall summer LWC mean was $5.02 \mu\text{g m}^{-3}$ and winter mean $2.22 \mu\text{g m}^{-3}$.

The diurnal variation of LWC contributed by W_i and W_o , along with total measured water, ambient T, RH, and solar radiation at CTR is shown in Figure 7. Predicted and measured LWC trends are in good overall agreement, although the largest discrepancy was observed during the daytime when LWC level was low and more difficult to measure and accurately predict. Nighttime RH median values were between 85% and 90% and resulted in significant water uptake that reached a peak just after sunrise near 7:30 am (local time). The dramatic peak in LWC starting at roughly 5:00 am, reaching a maximum between 7:30 and 8:00 am is likely due to RH increasing above 90%, at which point uptake of water rapidly increases with increasing RH. The similar rapid hygroscopic growths before sunrise were also observed at GIT, RS, and JST (Nov). After sunrise, rising temperatures lead to a rapid drop in RH, resulting in rapid loss of particle water. LWC reached lowest levels in the afternoon $\sim 2 \mu\text{g m}^{-3}$, only 20% of the peak value. W_o varied more than W_i ; W_o diurnal variation ratio (max/min) was 13.1 compared to 4.1 for W_i .

608 W_o was significant, accounting for on average 29-39% of the total $PM_{2.5}$ particle water for all our sites
609 (Figure 812 and Table 3). Note that, W_o at SCAPE sites were calculated by in-situ AMS
610 ~~measurement~~ measurements at each SCAPE site and ~~measured the mean~~ κ_{org} ~~mean~~ (0.126) measured at
611 CTR, due to lack of CCNc. Note that ϵ_{W_o} could be higher or lower at each site depending on the type of
612 organics presented and the related κ_{org} . Figure 812 shows that W_o is related to the organic mass fraction.
613 W_o is comparable to W_i at night. In contrast, it was only 33% of W_i during the daytime (Figure 73). The
614 significant fraction, even during daytime, indicates organic aerosol components will have a considerable
615 contribution to aerosol radiative forcing. Although organics are less hygroscopic than ammonium sulfate,
616 a large fraction of the $PM_{2.5}$ (~70%) was organic, making W_o contributions important. Of the organic
617 factors associated with W_o , ~~Cerully et al. (2014)~~ Cerully et al. (2014) showed that MO-OOA (more-
618 oxidized oxygenated organic aerosol, also referred to as LVOOA, low-volatile oxygenated organic
619 aerosol) and Isoprene-OA (isoprene derived organic aerosol) were twice as hygroscopic as LO-OOA
620 (less-oxidized oxygenated organic aerosol, also referred to as SVOOA, semi-volatile oxygenated organic
621 aerosol). The LWC associated with MO-OOA and Isoprene-OA account for ~60% and ~30% of total W_o
622 in the daytime, respectively.

623 **4.5 Ammonia partitioning, model validation and pH bias when gas/particle data not included**

624 ~~As noted earlier, ISORROPIA-II calculations at CTR for the SOAS study were evaluated by comparing~~
625 ~~measured and predicted $NH_{3(g)}$. Although NH_4 and $NH_{3(g)}$, along with other aerosol components, are input~~
626 ~~into the model, comparing ambient NH_4 and $NH_{3(g)}$ to model predictions is not a circular analyses. For~~
627 ~~each observed data point, the model calculates total ammonia from the NH_4 and $NH_{3(g)}$ input, and then~~
628 ~~calculates the gas-particle ammonia partitioning assuming equilibrium and the other various~~
629 ~~assumptions/limitations associated with the model. Figure 9 shows the SOAS study time series of~~
630 ~~measured and predicted $NH_{3(g)}$ and the fraction of ammonia in the gas phase ($NH_{3(g)}/(NH_{3(g)} + NH_{4(p)})$.~~
631 ~~Diurnal changes in the gas fraction can be seen and are likely due to diurnal changes in particle pH,~~
632 ~~discussed below.~~ The effect of aerosol sources of particle water on pH can also be delineated. pH
633 calculated just by W_i alone will be affected by an underestimation of particle water, resulting in a slightly
634 lower pH (Figure 13). W_o is on average 29% to 39% of total water at all sites, as a result pH increases by
635 0.15 to 0.23 units when W_o is included. Independent of the pH range, a 29% to 39% W_o fraction always
636 increases pH by 0.15 to 0.23 due to the logarithmic nature of pH. The effect of W_o on pH can be simply
637 denoted as $\log_{10}(1 - \epsilon_{W_o})$. For example, when ϵ_{W_o} is 90%, it shifts pH up by 1 unit. pH based on W_i is
638 highly correlated with pH for total water ($W_i + W_o$) (Slope = 0.94, intercept = -0.14, $R^2 = 0.97$). This
639 indicates that if organic mass and κ_{org} are not available, ISORROPIA-II run with only ion data will give

640 a reasonable estimate of pH, since both H_{air}^+ and W_i are outputs of ISORROPIA-II, while W_o is predicted
641 based on organic mass and κ_{org} . Accurate temperature and RH are still necessary inputs, especially when
642 RH is high.

643 4.4 Overall implications of low pH

644 Highly acidic aerosols throughout the southeast during all seasons Periods when almost all ammonia was
645 in the gas phase (ratio near 1) are related to precipitation events (06/10, 06/24, 06/28, 07/03, 07/04) when
646 aerosol concentrations were very low. Not including these events, the study mean (\pm SD) fraction
647 ammonia in the gas phase was 0.41 (\pm 0.16) (median value is also 0.41). These results provide confidence
648 in ISORROPIA-II calculations of particle pH, and demonstrate the utility of including both measurements
649 of particle and gas phases in these types of studies.

650 When gas and particle data are not available, pH predictions are likely not as accurate (Hennigan et al.,
651 2014). Running ISORROPIA-II in the forward mode, but with only aerosol concentrations as input, may
652 result in a bias in predicted pH due to repartitioning of ammonia in the model. In the southeast, where pH
653 is largely driven by SO_4 and NH_4 , the aerosol NH_4 input will be partitioned in the model between gas and
654 particle phases to establish equilibrium. Sulfate repartitioning does not occur since it is non-volatile.
655 Thus NH_4 will be lost from the particle and a lower pH predicted. At CTR ammonia partitioning has been
656 included in all model runs, but as no $\text{NH}_3(g)$ was available for SCAPE, the pH is likely biased at these sites
657 by roughly -1. In the following, all pHs reported for SCAPE are corrected for this bias (i.e., pH increased
658 by 1). Note that ammonia partitioning does not significantly affect the LWC prediction (W_i predicted
659 without $\text{NH}_3(g)$ vs W_i predicted with $\text{NH}_3(g)$, slope = 1.00, intercept = $-0.01 \mu\text{g m}^{-3}$, $R^2 = 0.98$).

660 4.6 pH diurnal, seasonal, and spatial trends in the southeast

661 At CTR, the aerosol was highly acidic, with predicted mean pH = 0.94 ± 0.59 (\pm SD). The minimum and
662 maximum pH were 0.94 and 2.23 respectively, and pH varied by approximately 1 on average throughout
663 the day (Figure 10). That is, the $H_{\text{aerosol}}^+/\text{LWC}$ ratio increased by a factor of 10 from night to day. LWC
664 max/min ratio was 5, whereas H^+ diurnal variation was significantly less (Figure 10), indicating that the
665 diurnal pattern in pH was driven mainly by particle water dilution. This is further demonstrated in Figure
666 11, which shows the diurnal variation in the NH_4/SO_4 molar ratio (the main ions driving pH), with only
667 slightly lower ratios during the day. The study mean (\pm SD) NH_4/SO_4 molar ratio was $1.4 (\pm 0.5)$. As
668 LWC is mainly controlled by RH and temperature, the pH diurnal variation was thus largely driven by
669 meteorological conditions, not aerosol composition. Because of this, a simple ion balance or per volume
670 air concentration of aerosol hydronium ion (H_{aerosol}^+) alone cannot be used as a proxy for pH in the particle.

Particle water and Fine particle pH in the southeastern United States

671 ~~At the SCAPE sites, JST, YRK, CIT, and RS, summer mean pHs were between 1 and 1.3, similar to CTR~~
672 ~~(mean of 0.94). In winter the pHs (mean between 1.8 and 2.2) were higher by ~1 unit. Although LWC~~
673 ~~was higher in summer, which tends to dilute H^+ and increase pH, summer pH was lower due to higher~~
674 ~~ion (i.e., sulfate) concentrations (Table 3). Similar diurnal pH patterns were seen at all sites in all seasons~~
675 ~~and follow the diurnal variations of particle water (Figure 12). Overall the pH in the southeast is very low,~~
676 ~~between 1 and 2 (mean), in both rural and urban environments. pH values in summer at various sites were~~
677 ~~similar (1 to 1.3), suggesting a fairly homogeneous distribution of acidity due to spatially uniform sulfate~~
678 ~~in the southeastern US (Zhang et al., 2012). In winter the diurnal range in pH was roughly 2, while the~~
679 ~~diurnal range in summer was smaller, with pH varying by roughly 1.~~

680 ~~These acidic aerosols in the southeast~~ will affect a variety of processes. For example, aerosol acidity
681 strongly shifts the partitioning of $HNO_{3(g)}$ to the gas phase resulting in low nitrate aerosol levels in the
682 southeast during summer (the higher summertime temperature also plays a secondary role). Aerosol
683 acidity also impacts the gas-particle partitioning of semi-volatile organic acids. ~~(Note, organic acids are~~
684 ~~not considered in our model, under these acidic conditions (pH = 1) their contributions to the ion~~
685 ~~balance H^+ (hence pH) are expected to be negligible. Because the pK_a ($pK_a = -\log_{10} K_a$, K_a referred as~~
686 ~~acid dissociation constant) of trace organic acids are > 2 (e.g., pK_a of formic acid, one of the strongest~~
687 ~~organic acids, is 3.75, Bacarella et al. (1955)), low pH prevents dissociation of the organic acids. Since~~
688 ~~H^+ is involved in aqueous phase reactions, low pH can affect reaction rates by providing more protons.~~
689 Investigators have found that ~~isoprene~~ Isoprene-OA formation is acid-catalyzed and sulfuric acid
690 participates in the reaction as a proton donor in chamber studies (Surratt et al., 2007)(Surratt et al., 2007).
691 However, aerosol acidity ~~may appears~~ not to be ~~the~~ limiting factor ~~of isoprene~~ for Isoprene-OA formation
692 in the southeastern US, owing to the consistently very low pH (Karambelas et al., 2014; Xu et al.,
693 2014)(Karambelas et al., 2014; Xu et al., 2015). Finally, low pH can affect the solubility of trace metals
694 ~~found in the insoluble fraction of aerosol~~ (e.g., mineral dust) such as Fe and Cu, which possibly increases
695 the toxicity of the redox metals (Ghio et al., 2012; Verma et al., 2014)(Ghio et al., 2012; Verma et al.,
696 2014) and may also have a long term effect on nutrient distributions in the region (Meskhidze et al., 2003;
697 Meskhidze et al., 2005Meskhidze et al., 2003; Meskhidze et al., 2005; Nenes et al., 2011Nenes et al.,
698 2011; Ito and Xu, 2014).

699 ~~Finally, the effect of aerosol sources of particle water on pH can also be delineated. pH calculated just by~~
700 ~~W_i alone will be affected by an underestimation of particle water, resulting in a slightly lower pH (Figure~~
701 ~~13). W_o is on average 29% to 39% of total water at all sites, as a result pH increases by 0.15 to 0.23 units~~
702 ~~when W_o is included. pH based on W_i is highly correlated with pH for total water ($W_i + W_o$) ($R^2 = 0.97$,~~
703 ~~Figure 14). This indicates that if organic mass and κ_{org} are not available, ISORROPIA-II run with only~~

Field Code Changed

704 ~~ion data will give a reasonable estimate of pH, since both H_{air}^+ and W_i are outputs of ISORROPIA-II,~~
705 ~~while W_o is predicted based on organic mass and κ_{org} . Accurate temperature and RH are still necessary~~
706 ~~inputs, especially when RH is high.~~

707 **5 Conclusions**

708 ~~Because particle pH is important and difficult to measure directly, by combining several models we~~
709 ~~present a comprehensive prediction method to calculate pH and include an uncertainty analysis.~~
710 ~~ISORROPIA-II is applied to calculate the concentration of H^+ and W_i from inorganic aerosol~~
711 ~~measurement, and CCN activity is used to predict W_o . The adjoint model of ISORROPIA,~~
712 ~~ANISORROPIA, is applied to determine sensitivities, which are used for propagating the measurement~~
713 ~~uncertainties to pH.~~

714 W_o Particle pH is important and difficult to measure directly. However, the commonly used pH proxies of
715 ion balances and NH_4^+/SO_4^{2-} molar ratios don't necessarily correlate with pH. Therefore, predicting pH is
716 the best method to analyze particle acidity. By combining several models we present a comprehensive
717 prediction method to calculate pH and include an uncertainty analysis. ISORROPIA-II is applied to
718 calculate the concentration of H_{air}^+ and W_i from inorganic aerosol measurements, and CCN activity is
719 used to predict W_o . The adjoint model of ISORROPIA, ANISORROPIA, is applied to determine
720 sensitivities, which are used for propagating the measurement uncertainties to pH. We find that W_o should
721 be included when predicting particle LWC when organic loadings are high (such as in the southeastern
722 US). However, the pH prediction is not highly sensitive to W_o , unless W_o mass fraction to the total
723 particle water is close to 1. Thus, in most cases particle pH can be predicted fairly accurately with just
724 measurements of inorganic species and ISORROPIA-II. However, constraining ISORROPIA-II with gas
725 phase species, such as $NH_{3(g)}$, as done in this work (or $HNO_{3(g)}$), is highly recommended, along with
726 running ISORROPIA-II in the forward mode. ISORROPIA-II does not consider organic acids, but at the
727 low pHs of this study, they do not contribute protons (Bacarella et al., 1955). However, for pH approaches
728 7, the dissociation of organic acids cannot be neglected. Finally, the model was validated through
729 comparing predicted to measured liquid water (W_i+W_o to $f(RH)$ water) and predicted to measured
730 $NH_{3(g)}$ concentrations.

731 On average, for the SOAS and SCAPE field studies, particle water associated with the $PM_{2.5}$ organic
732 species (W_o) accounted for a significant fraction of total LWC, at with a mean of 35% ($\pm 3\%$ SD) for
733 ~~SOAS and SCAPE field studies,~~ indicating the importance of organic hygroscopic properties to aerosol
734 ~~scattering~~ aqueous phase chemistry and direct radiative forcing in the southeast US. Although organics are

735 less hygroscopic than sulfate and ammonium, the larger mass fraction of organics than inorganics
736 promotes W_o uptake. Predicted LWC was compared to LWC determined from ambient versus dry light
737 scattering coefficients and a TEOM ~~measuring measurement of~~ dry $PM_{2.5}$ mass. In SOAS, ~~measured~~
738 ~~LWC the sum of W_i and W_o~~ was highly correlated and in close agreement with the ~~sum of W_i and W_o~~
739 ~~measured LWC~~ (slope = 0.91, ~~$rR^2 = 0.8775$~~). LWC showed a clear diurnal pattern, with a continuous
740 increase at night (median ~~nighttime LWC~~ of $10 \mu\text{g m}^{-3}$ ~~at 7:30 am~~) reaching a distinct peak when RH
741 reached a maximum near 90% just after sunrise ~~at during the period of~~ lowest ~~ambient daily~~ temperature,
742 followed by a rapid decrease and lower values during the day (median of $2 \mu\text{g m}^{-3}$ ~~at 2:30 pm~~).

743 In the southeastern US, pH normally ~~varies varied~~ from 0.5 to 2 in the summer and 1 to 3 in the winter,
744 indicating that the aerosol ~~is was highly~~ acidic throughout the year. The minimum and maximum pH were
745 -0.94 and 2.2 at CTR, respectively and varied from ~~a nighttime average of 1.5 at night to daytime average~~
746 ~~of 0.6 on average in the day~~, mostly attributable to diurnal variation in RH and temperature. Mean
747 ~~ammonium to sulfate~~ $\text{NH}_4^+/\text{SO}_4^{2-}$ molar ratios were 1.4 ± 0.5 (SD) and roughly half the ammonia was in
748 the gas phase ($\text{NH}_{3(g)} / (\text{NH}_{3(g)} + \text{NH}_{4(fp)}^+) = 41 \pm 16\%$, mean \pm SD). pH ~~throughout at other sites in~~ the
749 southeast (~~CTR excluded SCAPE study~~) was estimated based on a limited data set at an estimated
750 uncertainty of 9-49% and a systematic bias of -1 ~~if since~~ $\text{NH}_{3(g)}$ is not included in the thermodynamic
751 model run in ~~the~~ forward mode. pH can still be predicted with only aerosol measurements, but ~~an~~
752 ~~adjustment of~~ 1-unit pH increase ~~adjustment~~ is recommended for the southeastern US. pH has a diurnal
753 trend that follows LWC, higher (less acidic) at night and lower (more acidic) during the day. pH was also
754 generally higher in the winter (~ 2) than summer (~ 1). These low pHs have significant implications ~~on for~~
755 gas-aerosol partitioning, acid-catalyzed reactions including isoprene-OA formation, and trace metal
756 mobilization.

757 6 Acknowledgements

758 This work was supported by the NSF under grant number 1242258 as part of the SOAS campaign. GIT
759 SOAS Researchers were also supported by a US EPA STAR grant R835410 and NOAA CPO Award
760 NA100AR4310102. Measurements at other sites in the southeast were part of the EPA-supported SCAPE
761 Clean Air Center, made possible through US EPA grant R834799. The content of this publication are
762 solely the responsibility of the grantee and do not necessarily represent the official views of the US EPA.
763 Further, US EPA does not endorse the purchase of any commercial products or services mentioned in the
764 publication. SLC was supported by an appointment to the Research Participation Program at the Office of
765 Research and Development, US EPA, administered by ORISE. SHL acknowledges funding support from
766 NSF (AGS-1241498). AB acknowledges support within the framework of the Action ~~-~~Supporting

767 | Postdoctoral Researchers of the Operational Program "Education and Lifelong Learning" (Action's
768 | Beneficiary: General Secretariat for Research and Technology), and is co-financed by the European
769 | Social Fund (ESF) and the Greek State. We wish to thank the Southeastern Aerosol Research and
770 | Characterization (SEARCH) personnel for their many contributions supporting the field deployments.

771 | **References**

- 772 | Bacarella, A. L., Grunwald, E., Marshall, H. P., and Purlee, E. L.: The Potentiometric Measurement of
773 | Acid Dissociation Constants and pH in the System Methanol-Water. pK_a Values for Carboxylic
774 | Acids and Anilinium Ions, *J Org Chem*, 20, 747-762, 10.1021/Jo01124a007, 1955.
- 775 | [Bertram, A. K., Martin, S. T., Hanna, S. J., Smith, M. L., Bodsworth, A., Chen, Q., Kuwata, M., Liu, A.,
776 | You, Y., and Zorn, S. R.: Predicting the relative humidities of liquid-liquid phase separation,
777 | efflorescence, and deliquescence of mixed particles of ammonium sulfate, organic material, and
778 | water using the organic-to-sulfate mass ratio of the particle and the oxygen-to-carbon elemental
779 | ratio of the organic component. *Atmospheric Chemistry and Physics*, 11, 10995-11006,
780 | \[10.5194/acp-11-10995-2011\]\(#\), 2011.](#)
- 781 | Canagaratna, M. R., Jayne, J. T., Jimenez, J. L., Allan, J. D., Alfarra, M. R., Zhang, Q., Onasch, T. B.,
782 | Drewnick, F., Coe, H., Middlebrook, A., Delia, A., Williams, L. R., Trimborn, A. M., Northway,
783 | M. J., DeCarlo, P. F., Kolb, C. E., Davidovits, P., and Worsnop, D. R.: Chemical and
784 | microphysical characterization of ambient aerosols with the aerodyne aerosol mass spectrometer,
785 | *Mass spectrometry reviews*, 26, 185-222, 10.1002/mas.20115, 2007.
- 786 | Capps, S. L., Henze, D. K., Hakami, A., Russell, A. G., and Nenes, A.: ANISORROPIA: the adjoint of
787 | the aerosol thermodynamic model ISORROPIA, *Atmospheric Chemistry and Physics*, 12, 527-
788 | 543, 10.5194/acp-12-527-2012, 2012.
- 789 | Carlton, A. G., and Turpin, B. J.: Particle partitioning potential of organic compounds is highest in the
790 | Eastern US and driven by anthropogenic water, *Atmospheric Chemistry and Physics*, 13, 10203-
791 | 10214, 10.5194/acp-13-10203-2013, 2013.
- 792 | Carrico, C. M., Rood, M. J., and Ogren, J. A.: Aerosol light scattering properties at Cape Grim, Tasmania,
793 | during the First Aerosol Characterization Experiment (ACE 1), *Journal of Geophysical Research*,
794 | 103, 16565, 10.1029/98jd00685, 1998.
- 795 | Carrico, C. M., Rood, M. J., Ogren, J. A., Neususs, C., Wiedensohler, A., and Heintzenberg, J.: Aerosol
796 | optical properties at Sagres, Portugal during ACE-2, *Tellus B*, 52, 694-715, DOI 10.1034/j.1600-
797 | 0889.2000.00049.x, 2000.
- 798 | Cerully, K. M., Bougiatioti, A., Hite Jr, J. R., Guo, H., Xu, L., Ng, N. L., Weber, R., and Nenes, A.: On
799 | the link between hygroscopicity, volatility, and oxidation state of ambient and water-soluble
800 | aerosol in the Southeastern United States, *Atmospheric Chemistry and Physics Discussions*, 14,
801 | 30835-30877, 10.5194/acpd-14-30835-2014, 2014.
- 802 | Clegg, S. L., Brimblecombe, P., and Wexler, A. S.: Thermodynamic model of the system $H^+ - NH_4^+ - SO_4^{2-} -$
803 | $NO_3^- - H_2O$ at tropospheric temperatures, *J Phys Chem A*, 102, 2137-2154, Doi 10.1021/JP973042r,
804 | 1998.
- 805 | Czoschke, N. M., and Jang, M.: Acidity effects on the formation of α -pinene ozone SOA in the presence
806 | of inorganic seed, *Atmospheric Environment*, 40, 4370-4380, 10.1016/j.atmosenv.2006.03.030,
807 | 2006.
- 808 | DeCarlo, P. F., Kimmel, J. R., Trimborn, A., Northway, M. J., Jayne, J. T., Aiken, A. C., Gonin, M.,
809 | Fuhrer, K., Horvath, T., Docherty, K. S., Worsnop, D. R., and Jimenez, J. L.: Field-deployable,
810 | high-resolution, time-of-flight aerosol mass spectrometer, *Analytical chemistry*, 78, 8281-8289,
811 | 10.1021/ac061249n, 2006.

- 812 Eddingsaas, N. C., VanderVelde, D. G., and Wennberg, P. O.: Kinetics and Products of the Acid-
813 Catalyzed Ring-Opening of Atmospherically Relevant Butyl Epoxy Alcohols, *J Phys Chem A*,
814 114, 8106-8113, Doi 10.1021/Jp103907c, 2010.
- 815 Edney, E. O., Kleindienst, T. E., Jaoui, M., Lewandowski, M., Offenberg, J. H., Wang, W., and Claeys,
816 M.: Formation of 2-methyl tetrols and 2-methylglyceric acid in secondary organic aerosol from
817 laboratory irradiated isoprene/NO_x/SO₂/air mixtures and their detection in ambient PM_{2.5} samples
818 collected in the eastern United States, *Atmospheric Environment*, 39, 5281-5289,
819 10.1016/j.atmosenv.2005.05.031, 2005.
- 820 Engelhart, G. J., Asa-Awuku, A., Nenes, A., and Pandis, S. N.: CCN activity and droplet growth kinetics
821 of fresh and aged monoterpene secondary organic aerosol, *Atmospheric Chemistry and Physics*, 8,
822 3937-3949, 2008.
- 823 [Ervens, B., Turpin, B. J., and Weber, R. J.: Secondary organic aerosol formation in cloud droplets and](#)
824 [aqueous particles \(aqSOA\): a review of laboratory, field and model studies, *Atmospheric*](#)
825 [Chemistry and Physics Discussions](#), 11, 22301-22383, 10.5194/acpd-11-22301-2011, 2011.
- 826 Fountoukis, C., and Nenes, A.: ISORROPIA II: a computationally efficient thermodynamic equilibrium
827 model for K⁺-Ca²⁺-Mg²⁺-NH₄⁺-Na⁺-SO₄²⁻-NO₃⁻-Cl⁻-H₂O aerosols, *Atmospheric Chemistry and*
828 *Physics*, 7, 4639-4659, 2007.
- 829 Fountoukis, C., Nenes, A., Sullivan, A., Weber, R., Van Reken, T., Fischer, M., Matias, E., Moya, M.,
830 Farmer, D., and Cohen, R. C.: Thermodynamic characterization of Mexico City aerosol during
831 MILAGRO 2006, *Atmospheric Chemistry and Physics*, 9, 2141-2156, 2009.
- 832 [Frosch, M., Bilde, M., DeCarlo, P. F., Jurányi, Z., Tritscher, T., Dommen, J., Donahue, N. M., Gysel, M.,](#)
833 [Weingartner, E., and Baltensperger, U.: Relating cloud condensation nuclei activity and oxidation](#)
834 [level of α-pinene secondary organic aerosols, *Journal of Geophysical Research: Atmospheres*,](#)
835 [116, 10.1029/2011jd016401, 2011.](#)
- 836 Gao, S., Keywood, M., Ng, N. L., Surratt, J., Varutbangkul, V., Bahreini, R., Flagan, R. C., and Seinfeld,
837 J. H.: Low-molecular-weight and oligomeric components in secondary organic aerosol from the
838 ozonolysis of cycloalkenes and alpha-pinene, *J Phys Chem A*, 108, 10147-10164, Doi
839 10.1021/Jp047466e, 2004.
- 840 Ghio, A. J., Carraway, M. S., and Madden, M. C.: Composition of air pollution particles and oxidative
841 stress in cells, tissues, and living systems, *Journal of toxicology and environmental health. Part B*,
842 *Critical reviews*, 15, 1-21, 10.1080/10937404.2012.632359, 2012.
- 843 Hansen, D. A., Edgerton, E. S., Hartsell, B. E., Jansen, J. J., Kandasamy, N., Hidy, G. M., and Blanchard,
844 C. L.: The Southeastern Aerosol Research and Characterization Study: Part 1—Overview, *Journal*
845 *of the Air & Waste Management Association*, 53, 1460-1471, 10.1080/10473289.2003.10466318,
846 2003.
- 847 Hansen, D. A., Edgerton, E., Hartsell, B., Jansen, J., Burge, H., Koutrakis, P., Rogers, C., Suh, H., Chow,
848 J., Zielinska, B., McMurry, P., Mulholland, J., Russell, A., and Rasmussen, R.: Air Quality
849 Measurements for the Aerosol Research and Inhalation Epidemiology Study, *Journal of the Air &*
850 *Waste Management Association*, 56, 1445-1458, 10.1080/10473289.2006.10464549, 2006.
- 851 Hennigan, C. J., Bergin, M. H., Dibb, J. E., and Weber, R. J.: Enhanced secondary organic aerosol
852 formation due to water uptake by fine particles, *Geophysical Research Letters*, 35, L18801,
853 10.1029/2008gl035046, 2008.
- 854 Hennigan, C. J., ~~Nenes, A., and X, X.: In preparation, will edit this reference later as soon as Chris get the~~
855 ~~paper done!~~ [Izumi, J., Sullivan, A. P., Weber, R. J., and Nenes, A.: A critical evaluation of proxy](#)
856 [methods used to estimate the acidity of atmospheric particles, *Atmospheric Chemistry and*](#)
857 [Physics Discussions](#), 14, 27579-27618, 10.5194/acpd-14-27579-2014, 2014.
- 858 [Hildebrandt Ruiz, L., Paciga, A. L., Cerully, K., Nenes, A., Donahue, N. M., and Pandis, S. N.: Aging of](#)
859 [secondary organic aerosol from small aromatic VOCs: changes in chemical composition, mass](#)
860 [yield, volatility and hygroscopicity, *Atmospheric Chemistry and Physics Discussions*, 14, 31441-](#)
861 [31481, 10.5194/acpd-14-31441-2014, 2014.](#)

- 862 Iinuma, Y., Böge, O., Gnauk, T., and Herrmann, H.: Aerosol-chamber study of the α -pinene/O₃ reaction:
863 influence of particle acidity on aerosol yields and products, *Atmospheric Environment*, 38, 761-
864 773, 10.1016/j.atmosenv.2003.10.015, 2004.
- 865 IPCC: Climate Change 2013: The Physical Science Basis. Contribution of Working Group I to the Fifth
866 Assessment Report of the Intergovernmental Panel on Climate Change, Cambridge University
867 Press, Cambridge, United Kingdom and New York, NY, USA, 1535 pp., 2013.
- 868 Ito, A., and Xu, L.: Response of acid mobilization of iron-containing mineral dust to improvement of air
869 quality projected in the future, *Atmospheric Chemistry and Physics*, 14, 3441-3459, 10.5194/acp-
870 14-3441-2014, 2014.
- 871 Jang, M., Czoschke, N. M., Lee, S., and Kamens, R. M.: Heterogeneous atmospheric aerosol production
872 by acid-catalyzed particle-phase reactions, *Science*, 298, 814-817, 10.1126/science.1075798,
873 2002.
- 874 Karambelas, A., Pye, H. O. T., Budisulistiorini, S. H., Surratt, J. D., and Pinder, R. W.: Contribution of
875 Isoprene Epoxydiol to Urban Organic Aerosol: Evidence from Modeling and Measurements,
876 *Environmental Science & Technology Letters*, 1, 278-283, 10.1021/ez5001353, 2014.
- 877 Kim, J., Yoon, S.-C., Jefferson, A., and Kim, S.-W.: Aerosol hygroscopic properties during Asian dust,
878 pollution, and biomass burning episodes at Gosan, Korea in April 2001, *Atmospheric*
879 *Environment*, 40, 1550-1560, 10.1016/j.atmosenv.2005.10.044, 2006.
- 880 King, S. M., Rosenoern, T., Shilling, J. E., Chen, Q., and Martin, S. T.: Cloud condensation nucleus
881 activity of secondary organic aerosol particles mixed with sulfate, *Geophysical Research Letters*,
882 34, L24806, 10.1029/2007gl030390, 2007.
- 883 Kleindienst, T. E., Edney, E. O., Lewandowski, M., Offenberg, J. H., and Jaoui, M.: Secondary organic
884 carbon and aerosol yields from the irradiations of isoprene and α -pinene in the presence of NO_x
885 and SO₂, *Environmental science & technology*, 40, 3807-3812, Doi 10.1021/Es052446r, 2006.
- 886 Kotchenruther, R. A., and Hobbs, P. V.: Humidification factors of aerosols from biomass burning in
887 Brazil, *Journal of Geophysical Research*, 103, 32081, 10.1029/98jd00340, 1998.
- 888 Kuwata, M., Zorn, S. R., and Martin, S. T.: Using elemental ratios to predict the density of organic
889 material composed of carbon, hydrogen, and oxygen, *Environmental science & technology*, 46,
890 787-794, 10.1021/es202525q, 2012.
- 891 Lance, S., Nenes, A., Medina, J., and Smith, J. N.: Mapping the Operation of the DMT Continuous Flow
892 CCN Counter, *Aerosol Science and Technology*, 40, 242-254, 10.1080/02786820500543290,
893 2006.
- 894 Liao, H., and Seinfeld, J. H.: Global impacts of gas-phase chemistry-aerosol interactions on direct
895 radiative forcing by anthropogenic aerosols and ozone, *J Geophys Res-Atmos*, 110, D18208 Doi
896 10.1029/2005jd005907, 2005.
- 897 Liu, J., Zhang, X., Parker, E. T., Veres, P. R., Roberts, J. M., de Gouw, J. A., Hayes, P. L., Jimenez, J. L.,
898 Murphy, J. G., Ellis, R. A., Huey, L. G., and Weber, R. J.: On the gas-particle partitioning of
899 soluble organic aerosol in two urban atmospheres with contrasting emissions: 2. Gas and particle
900 phase formic acid, *Journal of Geophysical Research*, 117, D00V21, 10.1029/2012jd017912, 2012.
- 901 Magi, B. I., and Hobbs, P. V.: Effects of humidity on aerosols in southern Africa during the biomass
902 burning season, *Journal of Geophysical Research*, 108, 8495, Doi 10.1029/2002jd002144, 2003.
- 903 Malm, ~~G.-W. C., and Day, D.-E.-D.~~ ~~E.-D.~~: Estimates of aerosol species scattering characteristics as a function
904 of relative humidity, *Atmospheric Environment*, ~~2004-35, 2845-2860, DOI: 10.1016/S1352-~~
905 ~~2310(01)00077-2, 2001.~~
- 906 Meskhidze, N., Chameides, W. L., Nenes, A., and Chen, G.: Iron mobilization in mineral dust: Can
907 anthropogenic SO₂ emissions affect ocean productivity?, *Geophysical Research Letters*, 30, 2085
908 Doi 10.1029/2003gl018035, 2003.
- 909 Meskhidze, N., Chameides, W. L., and Nenes, A.: Dust and pollution: A recipe for enhanced ocean
910 fertilization?, *Journal of Geophysical Research*, 110, D03301, 10.1029/2004jd005082, 2005.

- 911 Mitchell, R. M., Campbell, S. K., Qin, Y., and Gras, J. L.: Performance Characteristics of Integrating
912 Nephelometers in the Australian Outback, *Journal of Atmospheric and Oceanic Technology*, 26,
913 984-995, 10.1175/2008jtecha1187.1, 2009.
- 914 Nemesure, S., Wagener, R., and Schwartz, S. E.: Direct shortwave forcing of climate by the
915 anthropogenic sulfate aerosol: Sensitivity to particle size, composition, and relative humidity, *J*
916 *Geophys Res-Atmos*, 100, 26105-26116, Doi 10.1029/95jd02897, 1995.
- 917 Nenes, A., Pandis, S. N., and Pilinis, C.: ISORROPIA: A new thermodynamic equilibrium model for
918 multiphase multicomponent inorganic aerosols, *Aquat Geochem*, 4, 123-152, Doi
919 10.1023/A:1009604003981, 1998.
- 920 Nenes, A., Krom, M. D., Mihalopoulos, N., Van Cappellen, P., Shi, Z., Bougiatioti, A., Zampas, P., and
921 Herut, B.: Atmospheric acidification of mineral aerosols: a source of bioavailable phosphorus for
922 the oceans, *Atmospheric Chemistry and Physics*, 11, 6265-6272, 10.5194/acp-11-6265-2011,
923 2011.
- 924 Nguyen, T. K. V., Petters, B., Coggon, M. D., Suda, S. M., Flagan, R. C., and Carlton, A. G.:
925 ~~Trends~~ Seinfeld, J. H.: Reactive uptake and photo-Fenton oxidation of glycolaldehyde in ~~partiele~~
926 ~~phase aerosol~~ liquid water during the Southern Oxidant and Aerosol Study, *Atmospheric*
927 *Chemistry and Physics Discussions*, 14, 7469-7516, *Environmental science & technology*, 47,
928 4307-4316, 10.5194/acpd-14-7469-2014, 2014 ~~1021/es400538j~~, 2013.
- 929 Nguyen, T. K. V., Petters, M. D., Suda, S. R., Guo, H., Weber, R. J., and Carlton, A. G.: Trends in
930 particle-phase liquid water during the Southern Oxidant and Aerosol Study, *Atmospheric*
931 *Chemistry and Physics*, 14, 10911-10930, 10.5194/acp-14-10911-2014, 2014.
- 932 Nowak, J. B., Huey, L. G., Russell, A. G., Tian, D., Neuman, J. A., Orsini, D., Sjostedt, S. J., Sullivan, A.
933 P., Tanner, D. J., Weber, R. J., Nenes, A., Edgerton, E., and Fehsenfeld, F. C.: Analysis of urban
934 gas phase ammonia measurements from the 2002 Atlanta Aerosol Nucleation and Real-Time
935 Characterization Experiment (ANARChE), *Journal of Geophysical Research*, 111, D17308,
936 10.1029/2006jd007113, 2006.
- 937 Orsini, D. A., Ma, Y., Sullivan, A., Sierau, B., Baumann, K., and Weber, R. J.: Refinements to the
938 particle-into-liquid sampler (PILS) for ground and airborne measurements of water soluble
939 aerosol composition, *Atmospheric Environment*, 37, 1243-1259, 10.1016/s1352-2310(02)01015-
940 4, 2003.
- 941 Pathak, R. K., Wang, T., Ho, K. F., and Lee, S. C.: Characteristics of summertime PM_{2.5} organic and
942 elemental carbon in four major Chinese cities: Implications of high acidity for water-soluble
943 organic carbon (WSOC), *Atmospheric Environment*, 45, 318-325,
944 10.1016/j.atmosenv.2010.10.021, 2011.
- 945 Petters, M. D., and Kreidenweis, S. M.: A single parameter representation of hygroscopic growth and
946 cloud condensation nucleus activity, *Atmospheric Chemistry and Physics*, 7, 1961-1971, 2007.
- 947 Pilinis, C., Pandis, S. N., and Seinfeld, J. H.: Sensitivity of Direct Climate Forcing by Atmospheric
948 Aerosols to Aerosol-Size and Composition, *J Geophys Res-Atmos*, 100, 18739-18754, Doi
949 10.1029/95jd02119, 1995.
- 950 Pye, H. O., Pinder, R. W., Piletic, I. R., Xie, Y., Capps, S. L., Lin, Y. H., Surratt, J. D., Zhang, Z., Gold,
951 A., Luecken, D. J., Hutzell, W. T., Jaoui, M., Offenberg, J. H., Kleindienst, T. E., Lewandowski,
952 M., and Edney, E. O.: Epoxide pathways improve model predictions of isoprene markers and
953 reveal key role of acidity in aerosol formation, *Environmental science & technology*, 47, 11056-
954 11064, 10.1021/es402106h, 2013.
- 955 Roberts, G. C., and Nenes, A.: A Continuous-Flow Streamwise Thermal-Gradient CCN Chamber for
956 Atmospheric Measurements, *Aerosol Science and Technology*, 39, 206-221,
957 10.1080/027868290913988, 2005.
- 958 Seinfeld, J. H., and Pandis, S. N.: *Atmospheric Chemistry and Physics: from Air Pollution to Climate*
959 *Change 2nd Edition*, John Wiley & Sons, Inc., Hoboken, New Jersey, 2006.

- 960 Sheridan, P. J., Jefferson, A., and Ogren, J. A.: Spatial variability of submicrometer aerosol radiative
961 properties over the Indian Ocean during INDOEX, *Journal of Geophysical Research*, 107, 8011,
962 Doi 10.1029/2000jd000166, 2002.
- 963 Sloane, C. S., Watson, J., Chow, J., Pritchett, L., and Richards, L. W.: Size-Segregated Fine Particle
964 Measurements by Chemical-Species and Their Impact on Visibility Impairment in Denver,
965 Atmospheric Environment. Part A. General Topics, 25, 1013-1024, Doi 10.1016/0960-
966 1686(91)90143-U, 1991.
- 967 [Song, M., Marcolli, C., Krieger, U. K., Zuend, A., and Peter, T.: Liquid-liquid phase separation and
968 morphology of internally mixed dicarboxylic acids/ammonium sulfate/water particles,
969 Atmospheric Chemistry and Physics, 12, 2691-2712, 10.5194/acp-12-2691-2012, 2012.](#)
- 970 [Song, M., Liu, P. F., Hanna, S. J., Martin, S. T., and Bertram, A. K.: Relative humidity-dependent
971 viscosities of isoprene-derived secondary organic material and atmospheric implications for
972 isoprene-dominant forests, Atmos. Chem. Phys. Discuss., 15, 1131-1169, 10.5194/acpd-15-1131-
973 2015, 2015.](#)
- 974 Sorooshian, A., Hersey, S., Brechtel, F. J., Corless, A., Flagan, R. C., and Seinfeld, J. H.: Rapid, Size-
975 Resolved Aerosol Hygroscopic Growth Measurements: Differential Aerosol Sizing and
976 Hygroscopicity Spectrometer Probe (DASH-SP), *Aerosol Science and Technology*, 42, 445-464,
977 10.1080/02786820802178506, 2008.
- 978 Stein, S. W., Turpin, B. J., Cai, X. P., Huang, C. P. F., and McMurry, P. H.: Measurements of Relative
979 Humidity-Dependent Bounce and Density for Atmospheric Particles Using the DMA-Impactor
980 Technique, *Atmospheric Environment*, 28, 1739-1746, Doi 10.1016/1352-2310(94)90136-8,
981 1994.
- 982 [Stokes, R. H., and Robinson, R. A.: Interactions in Aqueous Nonelectrolyte Solutions. I. Solute-Solvent
983 Equilibria, Journal of Physical Chemistry, 70, 2126-2130, Doi 10.1021/J100879a010, 1966.](#)
- 984 Surratt, J. D., Lewandowski, M., Offenberg, J. H., Jaoui, M., Kleindienst, T. E., Edney, E. O., and
985 Seinfeld, J. H.: Effect of acidity on secondary organic aerosol formation from isoprene,
986 *Environmental science & technology*, 41, 5363-5369, 2007.
- 987 Surratt, J. D., Chan, A. W., Eddingsaas, N. C., Chan, M., Loza, C. L., Kwan, A. J., Hersey, S. P., Flagan,
988 R. C., Wennberg, P. O., and Seinfeld, J. H.: Reactive intermediates revealed in secondary organic
989 aerosol formation from isoprene, *Proceedings of the National Academy of Sciences of the United
990 States of America*, 107, 6640-6645, 10.1073/pnas.0911114107, 2010.
- 991 Tang, I. N.: Phase transformation and growth of aerosol particles composed of mixed salts, *Journal of
992 Aerosol Science*, 7, 361-371, Doi 10.1016/0021-8502(76)90022-7, 1976.
- 993 Tang, I. N., and Munkelwitz, H. R.: Composition and Temperature-Dependence of the Deliquescence
994 Properties of Hygroscopic Aerosols, *Atmospheric Environment. Part A. General Topics*, 27, 467-
995 473, Doi 10.1016/0960-1686(93)90204-C, 1993.
- 996 Tanner, R. L., Olszyna, K. J., Edgerton, E. S., Knipping, E., and Shaw, S. L.: Searching for evidence of
997 acid-catalyzed enhancement of secondary organic aerosol formation using ambient aerosol data,
998 *Atmospheric Environment*, 43, 3440-3444, 10.1016/j.atmosenv.2009.03.045, 2009.
- 999 Tolocka, M. P., Jang, M., Ginter, J. M., Cox, F. J., Kamens, R. M., and Johnston, M. V.: Formation of
1000 oligomers in secondary organic aerosol, *Environmental science & technology*, 38, 1428-1434,
1001 2004.
- 1002 Turpin, B. J., and Lim, H.-J.: Species Contributions to PM_{2.5} Mass Concentrations: Revisiting Common
1003 Assumptions for Estimating Organic Mass, *Aerosol Science and Technology*, 35, 602-610,
1004 10.1080/02786820119445, 2001.
- 1005 Verma, V., Fang, T., Guo, H., King, L., Bates, J. T., Peltier, R. E., Edgerton, E., Russell, A. J., and Weber,
1006 R. J.: Reactive oxygen species associated with water-soluble PM_{2.5} in the southeastern United
1007 States: spatiotemporal trends and source apportionment, *Atmospheric Chemistry and Physics
1008 Discussions*, 14, 19625-19672, 10.5194/acpd-14-19625-2014, 2014.

- 1009 [Villani, P., Sellegri, K., Monier, M., and Laj, P.: Influence of semi-volatile species on particle](#)
1010 [hygroscopic growth, Atmospheric Environment, 79, 129-137, 10.1016/j.atmosenv.2013.05.069,](#)
1011 [2013.](#)
- 1012 Wexler, A. S., and Seinfeld, J. H.: Second-generation inorganic aerosol model, Atmospheric Environment.
1013 Part A. General Topics, 25, 2731-2748, Doi 10.1016/0960-1686(91)90203-J, 1991.
- 1014 Xu, L., Guo, H., Boyd, C. M., Klein, M., Bougiatioti, A., Cerully, K. M., Hite, J. R., Isaacman-VanWertz,
1015 G., Kreisberg, N. M., Knote, C., Olson, K., Koss, A., Goldstein, A. H., Hering, S. V., de Gouw, J-
1016 D., Baumann, K., Lee, S.-H., Nenes, A., Weber, R. J., and Ng, N. L.: Effects of **Anthropogenic**
1017 **Emissions** [anthropogenic emissions](#) on **Aerosol Formation** [aerosol formation](#) from
1018 **Isoprene** [isoprene](#) and **Monoterpenes** [monoterpenes](#) in the **Southeastern** [southeastern](#) United States,
1019 [P. Natl. Acad. Sci., 2014](#) [Proceedings of the National Academy of Sciences, 112, 37-42,](#)
1020 [10.1073/pnas.1417609112, 2015.](#)
- 1021 Yin, L., Niu, Z., Chen, X., Chen, J., Zhang, F., and Xu, L.: Characteristics of water-soluble inorganic ions
1022 in PM_{2.5} and PM_{2.5-10} in the coastal urban agglomeration along the Western Taiwan Strait Region,
1023 China, Environmental science and pollution research international, 21, 5141-5156,
1024 10.1007/s11356-013-2134-7, 2014.
- 1025 You, Y., Renbaum-Wolff, L., Carreras-Sospedra, M., Hanna, S. J., Hiranuma, N., Kamal, S., Smith, M. L.,
1026 Zhang, X., Weber, R. J., Shilling, J. E., Dabdub, D., Martin, S. T., and Bertram, A. K.: Images
1027 reveal that atmospheric particles can undergo liquid-liquid phase separations, Proceedings of the
1028 National Academy of Sciences of the United States of America, 109, 13188-13193,
1029 10.1073/pnas.1206414109, 2012.
- 1030 You, Y., [Renbaum-Wolff, L., and Bertram, A. K.: Liquid-liquid phase separation in particles containing](#)
1031 [organics mixed with ammonium sulfate, ammonium bisulfate, ammonium nitrate or sodium](#)
1032 [chloride, Atmospheric Chemistry and Physics, 13, 11723-11734, 10.5194/acp-13-11723-2013,](#)
1033 [2013.](#)
- 1034 [You, Y., Kanawade, V. P., de Gouw, J. A., Guenther, A. B., Madronich, S., Sierra-Hernández, M. R.,](#)
1035 [Lawler, M., Smith, J. N., Takahama, S., Ruggeri, G., Koss, A., Olson, K., Baumann, K., Weber,](#)
1036 [R. J., Nenes, A., Guo, H., Edgerton, E. S., Porcelli, L., Brune, W. H., Goldstein, A. H., and Lee, S.](#)
1037 [H.: Atmospheric amines and ammonia measured with a Chemical Ionization Mass Spectrometer](#)
1038 [\(CIMS\), Atmospheric Chemistry and Physics Discussions, 14, 16411-16450, 10.5194/acpd-14-](#)
1039 [16411-2014, 2014.](#)
- 1040 [Zdanovskii, A. B.: Trudy Solyanoi Laboratorii Akad. Nauk SSSR, 2, 1936.](#)
- 1041 Zhang, X., Liu, Z., Hecobian, A., Zheng, M., Frank, N. H., Edgerton, E. S., and Weber, R. J.: Spatial and
1042 seasonal variations of fine particle water-soluble organic carbon (WSOC) over the southeastern
1043 United States: implications for secondary organic aerosol formation, Atmospheric Chemistry and
1044 Physics, 12, 6593-6607, 10.5194/acp-12-6593-2012, 2012.
- 1045 [Zuend, A., Marcolli, C., Peter, T., and Seinfeld, J. H.: Computation of liquid-liquid equilibria and phase](#)
1046 [stabilities: implications for RH-dependent gas/particle partitioning of organic-inorganic aerosols,](#)
1047 [Atmospheric Chemistry and Physics, 10, 7795-7820, 10.5194/acp-10-7795-2010, 2010.](#)
- 1048 [Zuend, A., and Seinfeld, J. H.: Modeling the gas-particle partitioning of secondary organic aerosol: the](#)
1049 [importance of liquid-liquid phase separation, Atmospheric Chemistry and Physics, 12, 3857-3882,](#)
1050 [10.5194/acp-12-3857-2012, 2012.](#)

Formatted: Space After: 0 pt

Formatted: Line spacing: single

1054 **Table. 1.** Deployment status of instruments at various sites. All the listed instruments or probes were
 1055 operated at CTR for SOAS.

Site	Period (mm yyyy)	PILS-IC	AMS	CCNc	Nephelometer	TEOM	RH&T
JST	May&Nov 2012	NO	YES	NO	NO	YES	YES
YRK	Jul&Dec 2012	NO	YES	NO	NO	YES	YES
GIT	Jul-Aug 2012	NO	YES	NO	NO	YES	YES
RS	Sep Sept 2012	NO	YES	NO	NO	YES	YES
CTR	Jun-Jul 2013	YES	YES	YES	YES	YES	YES

1056

1057 **Table 2.** Sensitivity of $H^+H_{air}^+$ to ions from ANISORROPIA (2nd row) and contribution of uncertainty.
 1058 Uncertainties of inorganic ions ($\frac{\delta_{Ion}}{Ion}$) are calculated based on a combination of PILS-IC instrumental
 1059 relative uncertainties (IC uncertainty, referred to as $\frac{\delta_{Ion,IC}}{Ion}$, all estimated to be 15%) and the difference
 1060 between PILS-IC and AMS ($\frac{\delta_{Ion,IC-AMS}}{Ion}$, defined as the (slope - 1) in Figure 4a & 2b) (3rd row), where
 1061 $\frac{\delta_{Ion}}{Ion} = \sqrt{\left(\frac{\delta_{Ion,IC}}{Ion}\right)^2 + \left(\frac{\delta_{Ion,IC-AMS}}{Ion}\right)^2} \sqrt{\left(\frac{\delta_{Ion,IC}}{Ion}\right)^2 + \left(\frac{\delta_{Ion,IC-AMS}}{Ion}\right)^2}$ (4th row). Contribution of uncertainty is the
 1062 ratio of ion uncertainty over $H^+H_{air}^+$ uncertainty $\frac{\delta_{H^+}}{H^+} \frac{\delta_{H_{air}^+}}{H_{air}^+}$, calculated to be 14% in Equation 8) (5th row).

PILS-IC ion concentration, $\mu\text{g m}^{-3}$ (mean \pm SD)	SO ₄	NH ₄ ⁺	Na ⁺	NO ₃ ⁻	Cl ⁻
	1.73 \pm 1.21	0.46 \pm 0.34	0.03 \pm 0.07	0.08 \pm 0.08	0.02 \pm 0.03
Sensitivity (mean \pm SD)	$\frac{\partial H^+}{\partial SO_4} \left \frac{\partial H_{air}^+}{\partial SO_4} \right $	$\frac{\partial H^+}{\partial NH_4} \left \frac{\partial H_{air}^+}{\partial NH_4} \right $	$\frac{\partial H^+}{\partial Na} \left \frac{\partial H_{air}^+}{\partial Na} \right $	$\frac{\partial H^+}{\partial NO_3} \left \frac{\partial H_{air}^+}{\partial NO_3} \right $	$\frac{\partial H^+}{\partial Cl} \left \frac{\partial H_{air}^+}{\partial Cl} \right $
	0.51 \pm 0.34	0.32 \pm 0.31	0.19 \pm 0.27	0.002 \pm 0.007	0.000 \pm 0
$\frac{\delta_{Ion,IC-AMS}}{Ion}$	$\frac{\delta_{SO_4,IC-AMS}}{SO_4}$	$\frac{\delta_{NH_4,IC-AMS}}{NH_4} \frac{\delta_{NH_4,IC}}{NH_4}$	$\frac{\delta_{Na,IC-AMS}}{Na} \frac{\delta_{Na,IC}}{Na}$	$\frac{\delta_{NO_3,IC-AMS}}{NO_3} \frac{\delta_{NO_3,IC}}{NO_3}$	$\frac{\delta_{Cl,IC-AMS}}{Cl} \frac{\delta_{Cl,IC}}{Cl}$
	20.5%	1.5%	N/A*	**	**
$\frac{\delta_{Ion}}{Ion}$	$\frac{\delta_{SO_4}}{SO_4}$	$\frac{\delta_{NH_4}}{NH_4} \frac{\delta_{NH_4^+}}{NH_4^+}$	$\frac{\delta_{Na}}{Na} \frac{\delta_{Na^+}}{Na^+}$	$\frac{\delta_{NO_3}}{NO_3} \frac{\delta_{NO_3^-}}{NO_3^-}$	$\frac{\delta_{Cl}}{Cl} \frac{\delta_{Cl^-}}{Cl^-}$
	25.4%	15.1%	15%	15%	15%
Contribution to $H^+H_{air}^+$ uncertainty	$\frac{\delta_{H^+}}{H^+} \frac{\delta_{SO_4}}{SO_4} \left \frac{\partial H}{\partial S} \right $	$\frac{\delta_{H^+}}{H^+} \frac{\delta_{NH_4}}{NH_4} \left \frac{\partial H}{\partial N} \right $	$\frac{\delta_{H^+}}{H^+} \frac{\delta_{Na}}{Na} \left \frac{\partial H}{\partial N} \right $	$\frac{\delta_{H^+}}{H^+} \frac{\delta_{NO_3}}{NO_3} \left \frac{\partial H}{\partial N} \right $	$\frac{\delta_{H^+}}{H^+} \frac{\delta_{Cl}}{Cl} \left \frac{\partial H}{\partial Cl} \right $
	0.93	0.35	0.20	0.002	0.000

Formatted: Superscript
 Formatted: Superscript
 Formatted: Superscript
 Formatted: Superscript

1063 * Na⁺ is not measured by AMS.
 1064 ** $\frac{\partial H^+}{\partial NO_3} \left| \frac{\partial H_{air}^+}{\partial NO_3} \right|$ and $\frac{\partial H^+}{\partial Cl} \left| \frac{\partial H_{air}^+}{\partial Cl} \right|$ are less than 1% of the other $H^+H_{air}^+$ sensitivities, and the loadings of
 1065 NO₃⁻ and Cl⁻ are less than 5% of the total inorganic ion mass. As a result, their contributions to $H^+H_{air}^+$
 1066 uncertainty are negligible.

Particle water and Fine particle pH in the southeastern United States

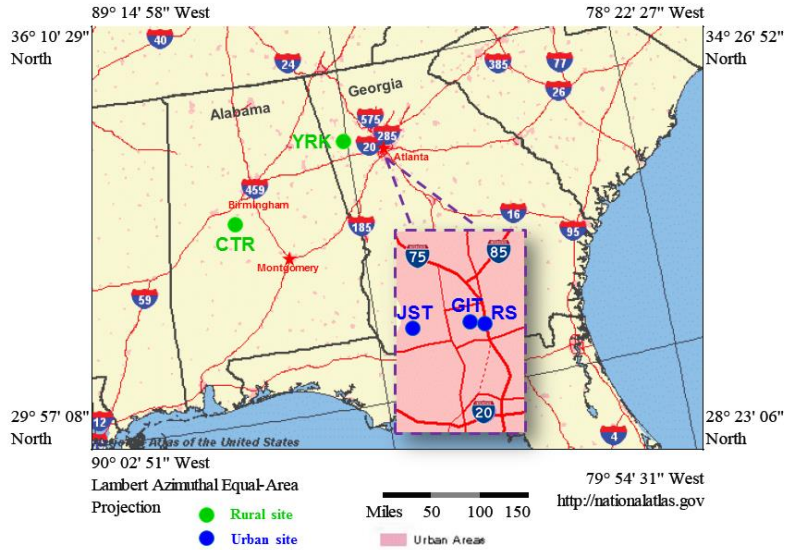
1068 **Table 3.** Water and pH prediction for SCAPE sites. Means and SDs are listed, if not specified. Total ion
 1069 concentration is counted as the sum of AMS inorganics (3rd row). $\epsilon(W_o)\epsilon_{W_o}$ is the mass fraction of W_o (5th
 1070 row).

	JST 05/2012	YRK 07/2012	GIT 08/2012	RS 09/2012	JST 11/2012	YRK 12/2012
RH, %	67 ± 19	66 ± 21	71 ± 17	72 ± 20	63 ± 19	73 ± 21
T, °C	23.1 ± 4.3	27.7 ± 4.4	26.3 ± 3.5	21.4 ± 3.8	11.5 ± 4.8	9.8 ± 5.2
Total ion concentration, $\mu\text{g m}^{-3}$	4.1 ± 2.1	4.5 ± 2.2	5.3 ± 2.6	4.1 ± 2.7	3.6 ± 2.1	2.3 ± 1.8
$\frac{\delta_{pH}}{pH}$ from 1.10RH	22.3%	21.4%	48.3%	22.1%	2.5%	1.4%
Total $\frac{\delta_{pH}}{pH}$	23.9%	23.0%	49.0%	23.7%	8.8%	8.6%
$\epsilon(W_o)\epsilon_{W_o}$ %	34 ± 11	37 ± 8	33 ± 10	38 ± 11	39 ± 16	29 ± 15
LWC, $\mu\text{g m}^{-3}$	5.98 ± 6.28	8.14 ± 8.47	8.41 ± 7.67	7.81 ± 9.23	5.88 ± 8.69	3.24 ± 3.46
pH*	1.3 ± 0.7	1.1 ± 0.6	1.1 ± 0.4	1.3 ± 0.7	2.2 ± 0.9	1.8 ± 1.0
LWC, $\mu\text{g m}^{-3}$ (median)	3.74 ± 6.28	5.29 ± 8.47	6.06 ± 7.67	4.31 ± 9.23	2.14 ± 8.69	2.02 ± 3.46
pH* (median)	1.2 ± 0.7	1.0 ± 0.6	1.0 ± 0.4	1.2 ± 0.7	2.3 ± 0.9	1.8 ± 1.0

1071 * A bias correction of 1 pH unit is applied due to not considering ammonia partitioning. [See Section 4.2c](#)
 1072 [for details.](#)

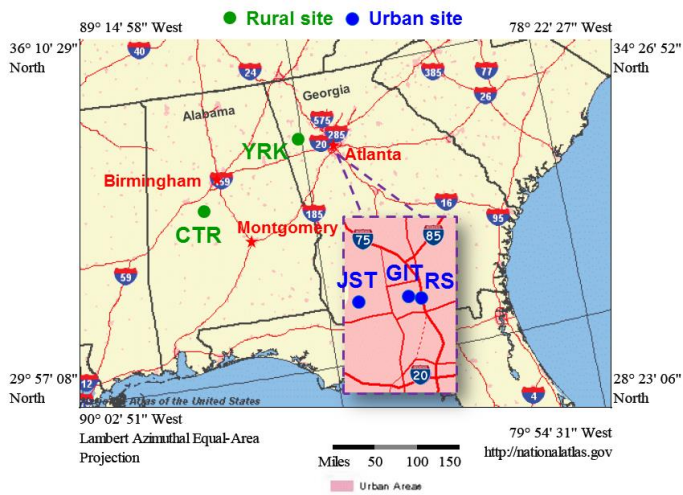
1073

Particle water and Fine particle pH in the southeastern United States



1074

1075



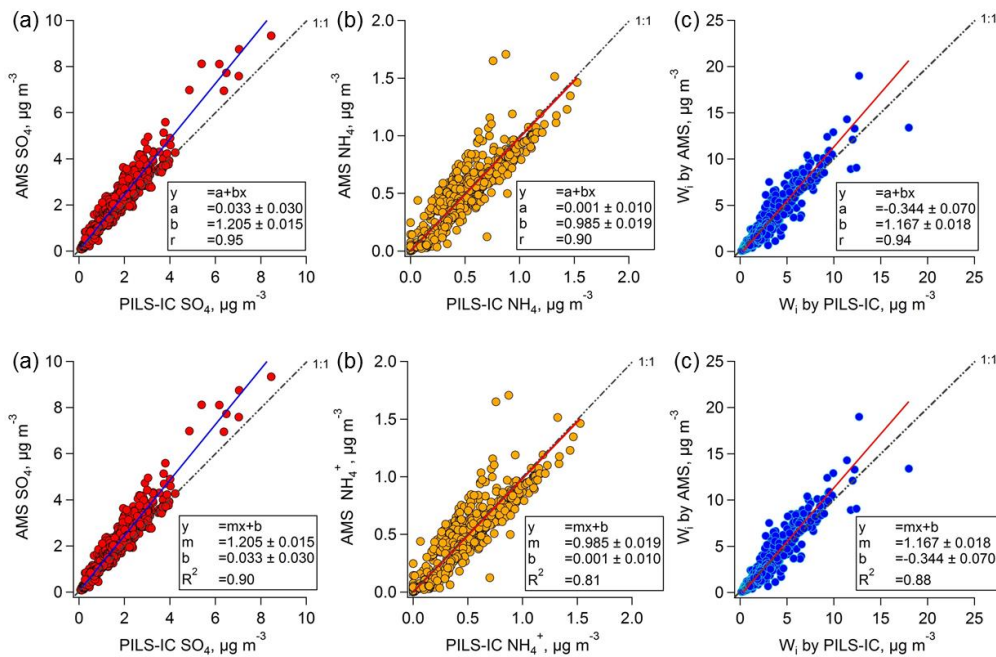
1076

1077

Fig. 1. Sampling sites in the southeastern USA, consisting of two rural and three urban sites.

1078

1079



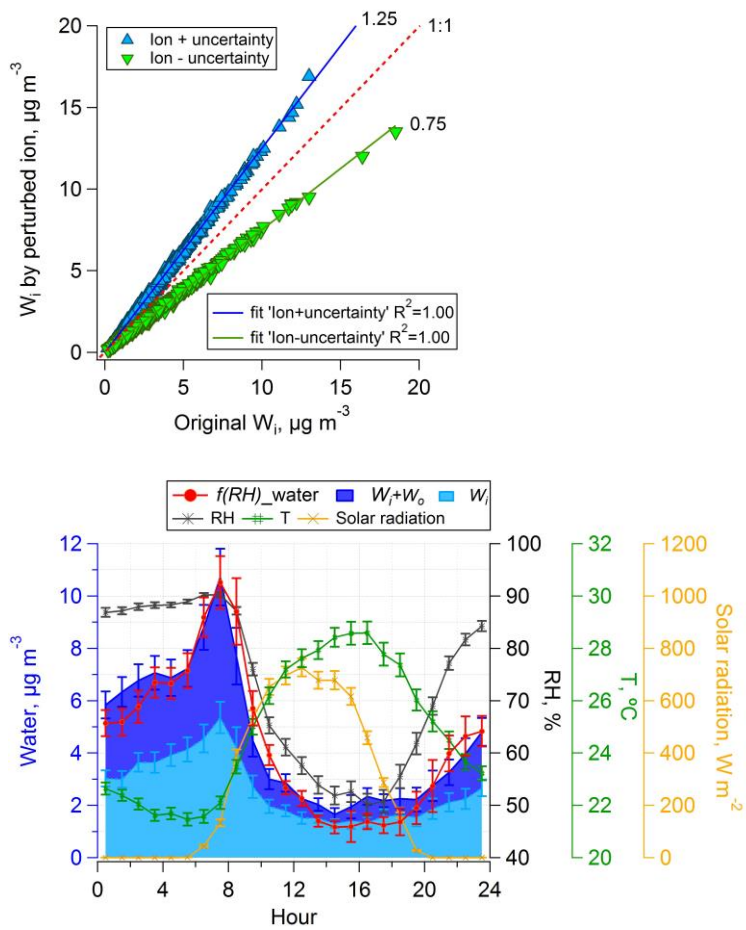
1080

1081 **Fig. 2.** Comparisons of PM_{10} AMS sulfate, ammonium to PM_{10} and $\text{PM}_{2.5}$ PILS-IC (i.e. complete SOAS
 1082 study) and predicted W_i . Orthogonal distance regression (ODR) fits were applied.

1083

Formatted: None

1084

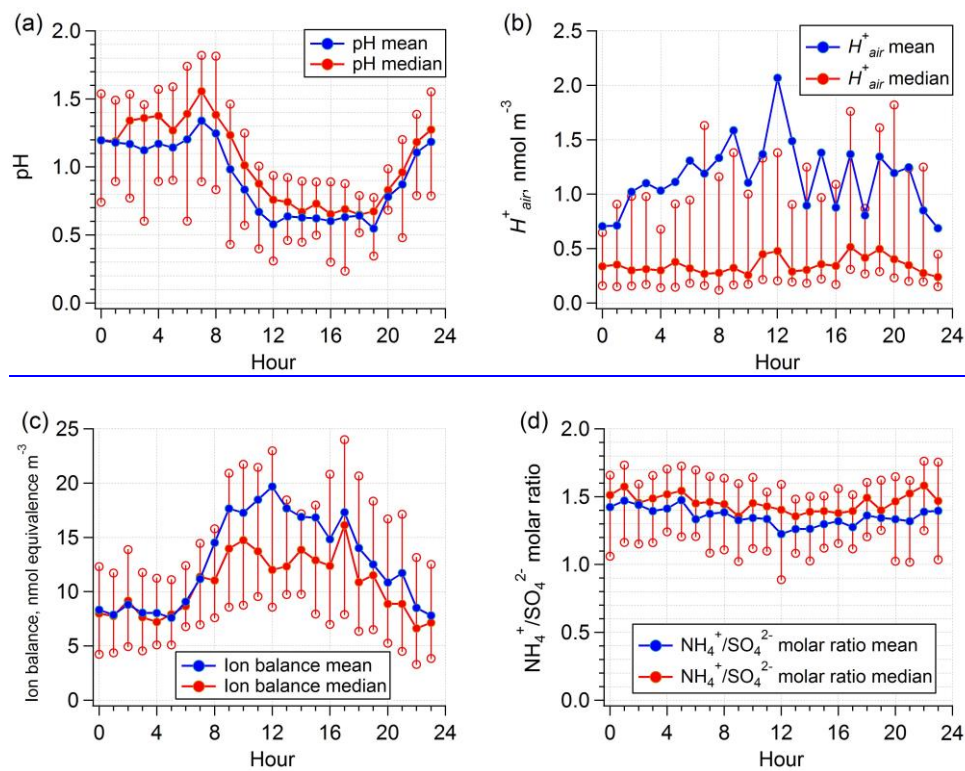


1085

1086 **Fig. 3.** CTR (SOAS) diurnal profiles of predicted and measured water, measured RH, T, and solar
1087 radiation. Median hourly averages are shown and standard errors are plotted as error bars.

1088

Formatted: Font: Not Bold

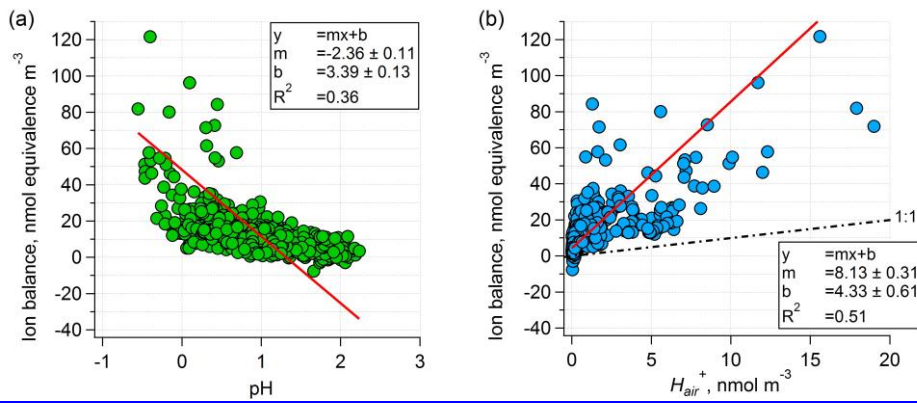


1089

1090

1091 **Fig. W4.** CTR (SOAS) diurnal patterns of calculated pH based on ~~artificially-perturbed~~total predicted
1092 water ($W_i + W_o$) (a), H^+_{air} predicted by ISORROPIA-II (b), ion balance (c), and NH_4^+/SO_4^{2-} molar ratio
1093 (d). Mean and median values are shown, together with 25% and 75% quantiles marked as non-filled
1094 circles.

1095



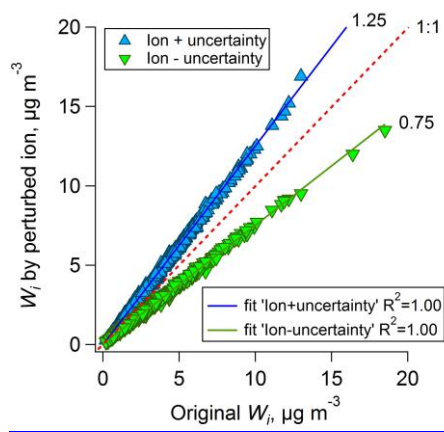
1096

1097 [Fig. 5. Comparison of ion balance to pH \(a\) and to \$H_{air}^+\$ \(b\) at CTR \(SOAS\). An ODR fit was applied.](#)

1098

1099

1100

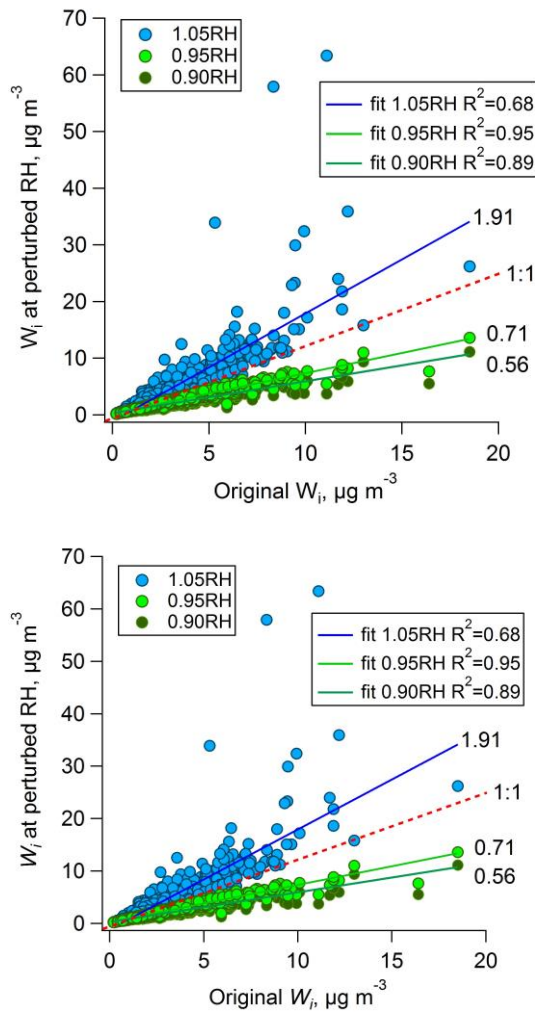


1101

1102 [Fig. 6.](#) W_i based on artificially perturbed ion data at upper and lower uncertainty limits is compared to W_i

1103 [at base level.](#) The slopes indicate [the](#) W_i uncertainty caused by ions.

1104



1105

1106

1107

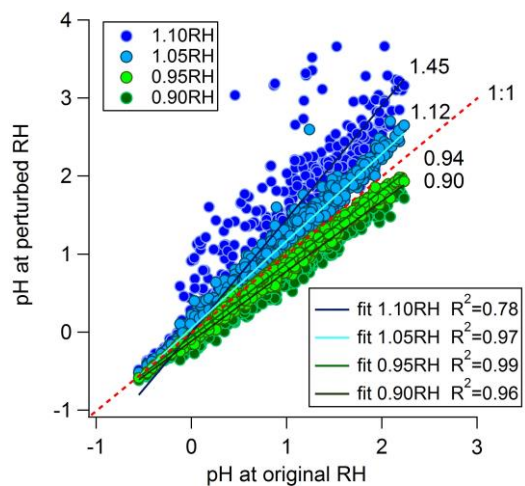
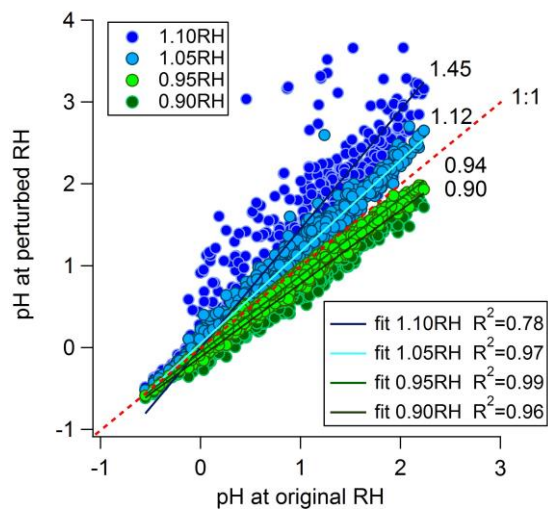
1108

1109

1110

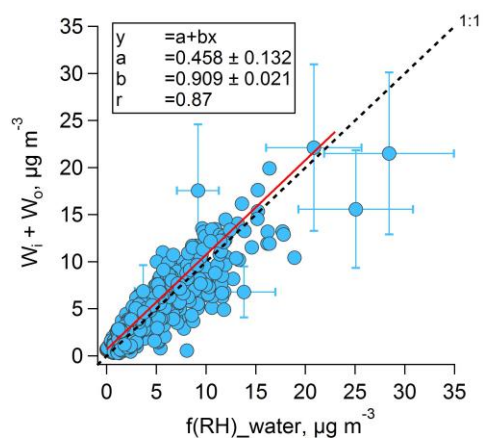
1111

Fig. 47. W_i based on artificially perturbed RH at upper and lower uncertainty limits compared to W_i at base level. 1.10RH (i.e., RH increased by 10%) is not plotted because it results in much larger W_i than the rest. Slopes and R^2 indicate corresponding W_i uncertainty caused by variability (uncertainty) in RH.



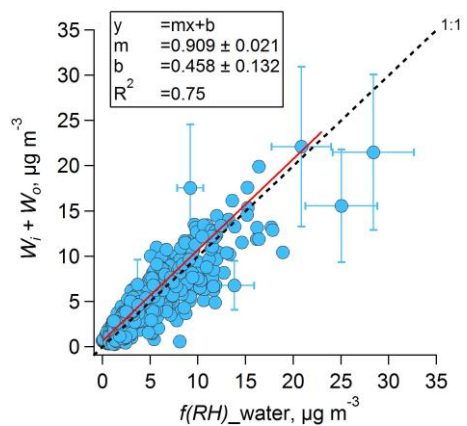
1114 **Fig. 58.** pH predictions by perturbed perturbing RH compared to pH at base level. W_i , W_o , and H_{air}^+ were
 1115 recalculated based on $\pm 5\%$ and $\pm 10\%$ original RH to investigate pH uncertainty. The slopes and R^2
 1116 indicate pH uncertainty caused by RH.

1117



1118

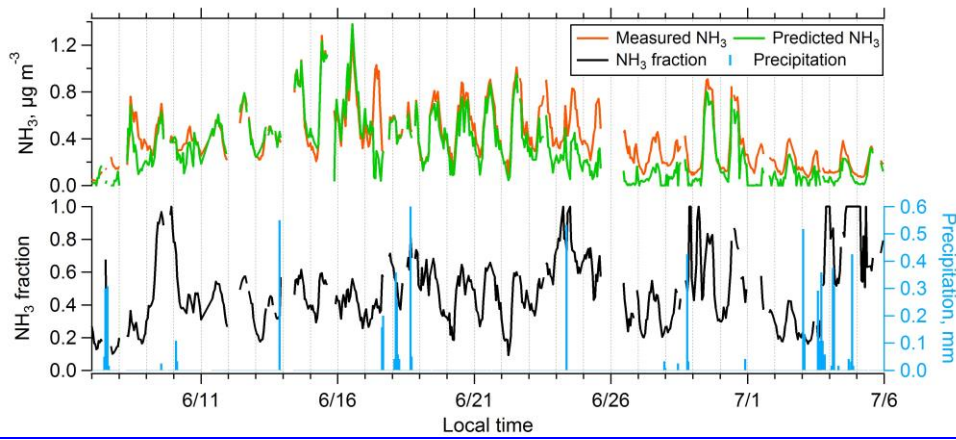
1119



1120

1121 **Fig. 69.** Comparison between total predicted and measured water by nephelometers based on hourly
1122 averaged data at CTR (SOAS). An ODR fit was applied. Error bars for selected points are shown.

1123

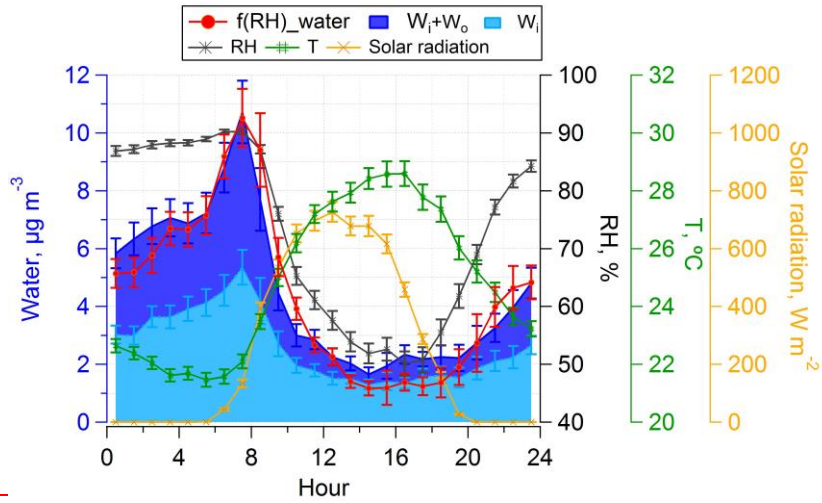


1124

1125 Fig. 10.

1126

1127

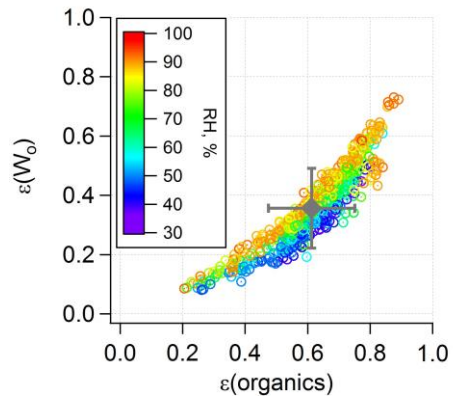


1128

1129 ~~Fig. 7. CTR (SOAS) diurnal profiles of predicted and measured water, measured RH, T, and solar~~

1130 ~~radiation. Median hourly averages and standard error plotted as error bars at local hour are shown.~~

1131



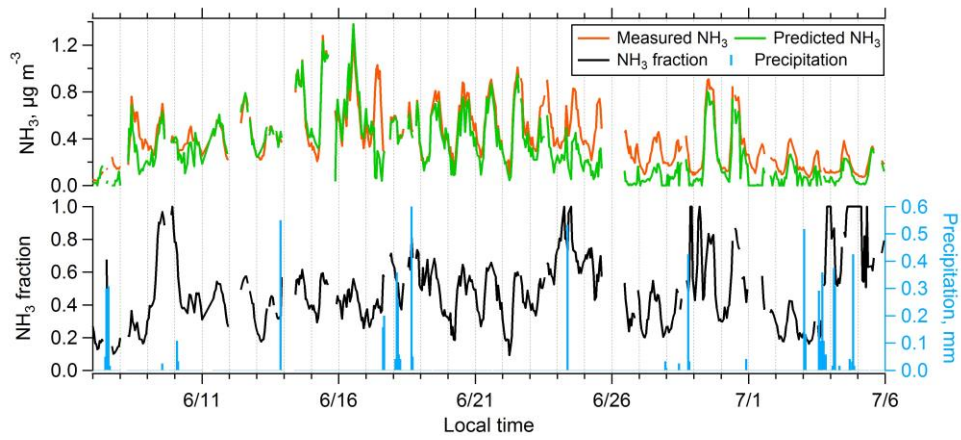
1132

1133

1134

1135

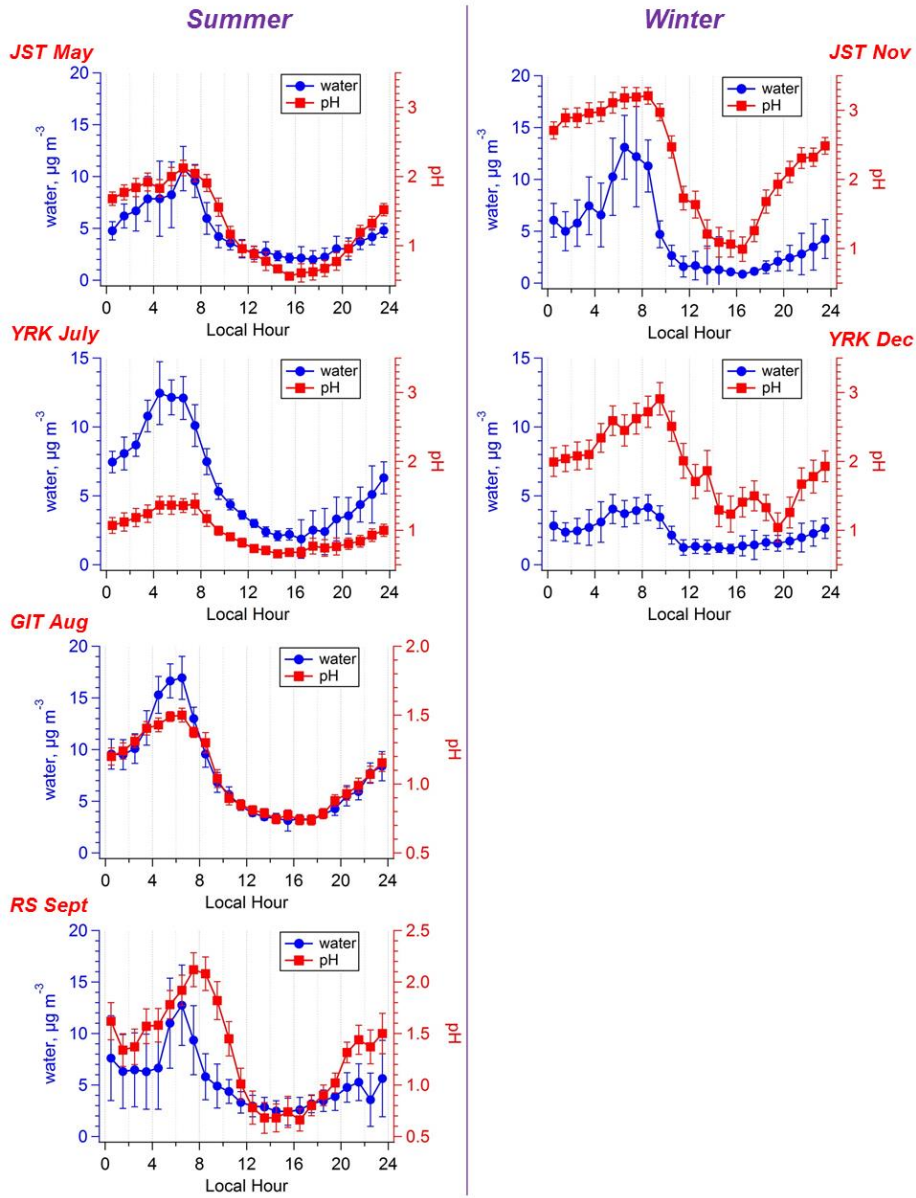
~~Fig. 8. W_o fraction plotted with organic mass fraction at CTR (SOAS). Overall study mean and standard deviation is also shown. $\epsilon_{\text{organe}} = 61 \pm 14\%$ and $\epsilon_{\text{w}} = 36 \pm 14\%$.~~



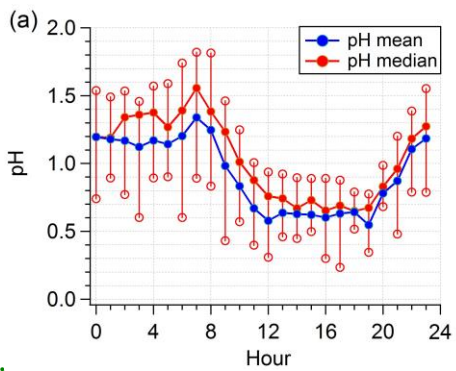
1136

1137 **Fig. 9.** CTR (SOAS) time series of hourly averaged measured $\text{NH}_{3(g)}$, predicted $\text{NH}_{3(g)}$, $\text{NH}_{3(g)}$ fraction
1138 (i.e., measured $\text{NH}_{3(g)} / (-\text{NH}_{3(g)} + \text{NH}_{4(\text{aq})}^+)$) and precipitation.

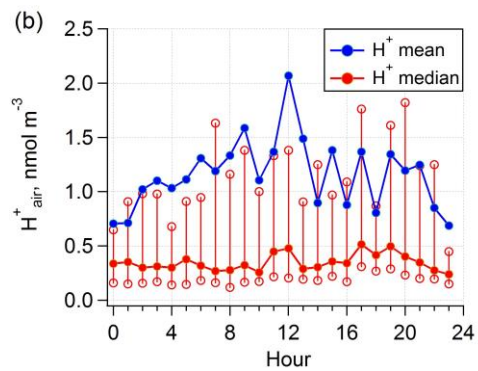
1139



1140



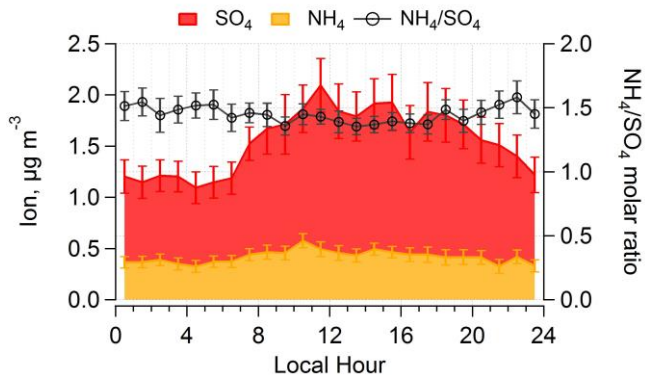
1141 **Fig. 11.**



1142 **Fig. 10.** CTR (SOAS) diurnal patterns of calculated pH based on total predicted water ($W_t + W_p$) and H^+
1143 predicted by ISORROPIA-II. Mean and median values are shown, together with 25% and 75% quantiles
1144 marked as non-filled circles.
1145

1146

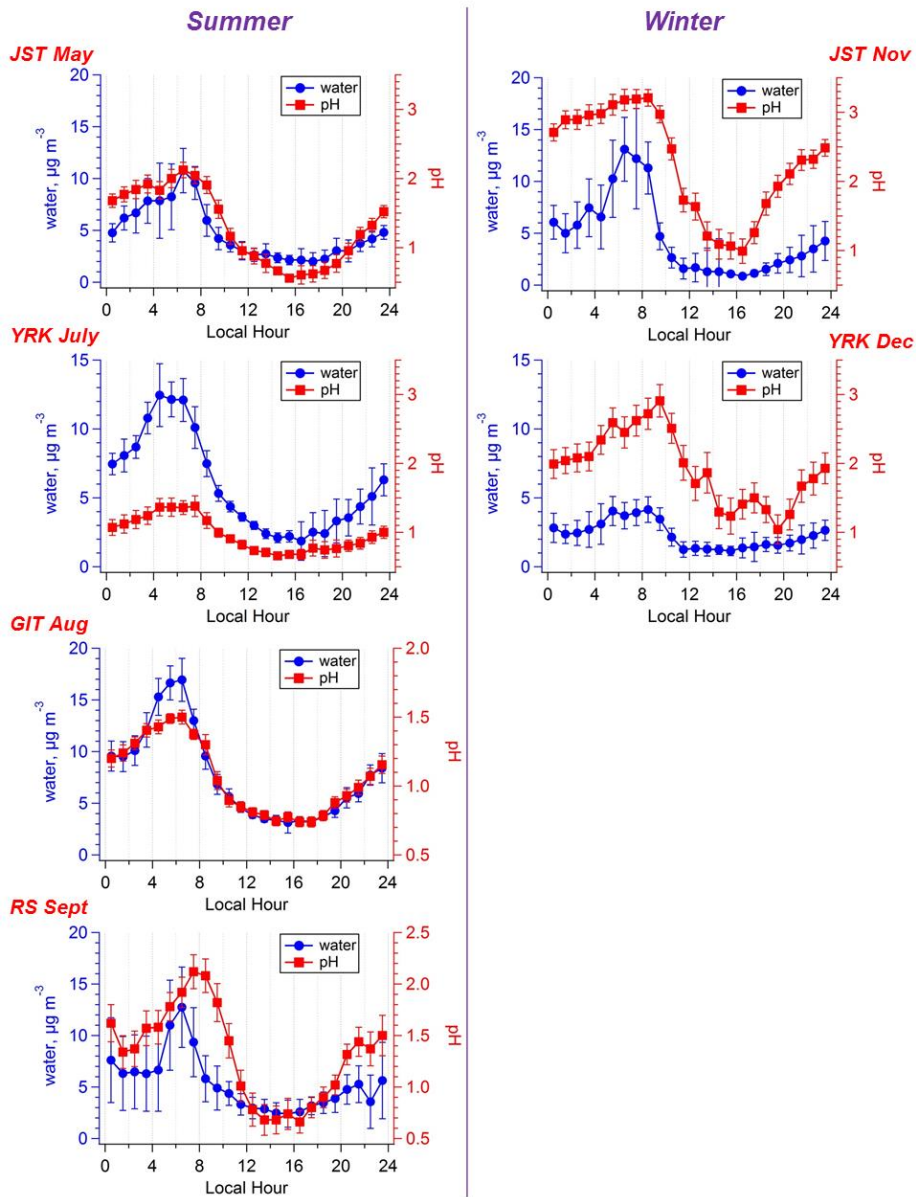
1147



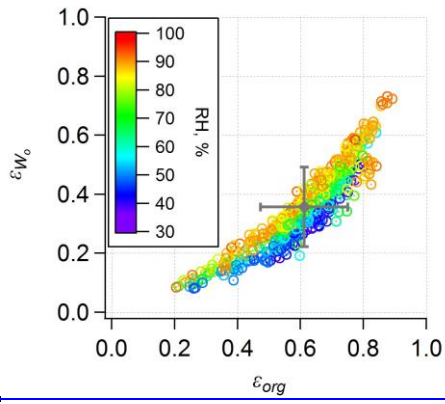
1148

1149 **Fig. 11** CTR (SOAS) diurnal patterns of PLS-IC NH_4 and SO_4 , and the molar ratio. Median hourly
1150 averages and standard error bars at local hours are plotted.

1151



1152
 1153 **Fig. 12.** LWC and pH diurnal variation at SCAPE sites: comparison between summer and winter. Median
 1154 hourly averages and standard error bars at local hour are plotted. A bias correction of 1 pH unit is applied
 1155 due to not considering ammonia partitioning.

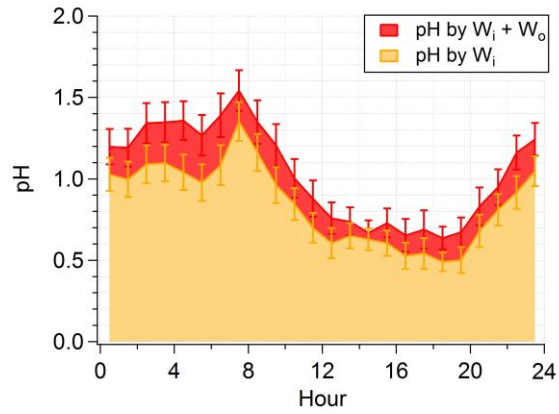


1156

1157

Fig. 12.

Particle water and Fine particle pH in the southeastern United States

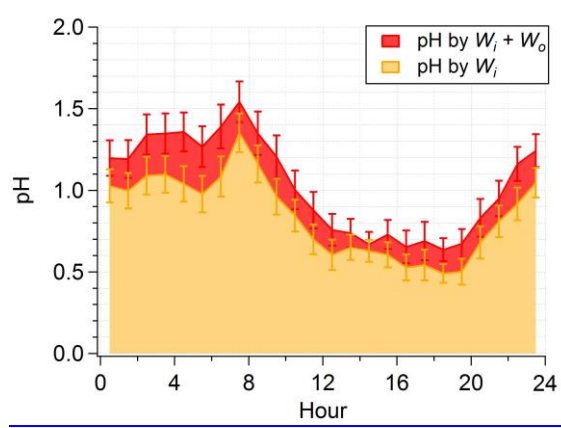


1158

1159 W_o mass fraction (ϵ_{W_o}) plotted versus organic mass fraction at CTR (SOAS). Overall study mean and

1160 standard deviation is also shown. $\epsilon_{Org} = 61 \pm 14\%$ and $\epsilon_{W_o} = 36 \pm 14\%$.

1161

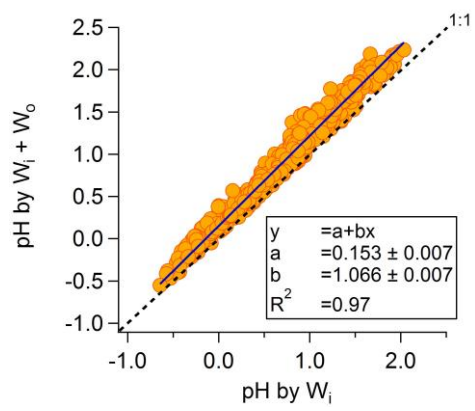


1162

1163 **Fig. 13.** CTR (SOAS) pH diurnal profiles based on total predicted water and W_i , respectively. Median

1164 hourly averages and standard error bars at local hour are plotted.

1165



1166

1167

1168

Fig. 14. Comparison between pH based on W_i and pH based on total predicted water at CTR (SOAS). An ODR fit was applied.